MSc Thesis Report

Methanol as a Hydrogen Carrier Coupled with Magnesium-Based Oxides Carbonation for Carbon Dioxide Capture

Submitted by

Sara Zallaya
Chemical and Process Engineering
University of Twente | TNW Faculty

Under the guidance of

Chair: Prof.dr. S.R.A. Kersten (Sascha)
Tutor: Dr.ir. A.G.J. van der Ham (Louis)
Member: Prof.dr.ir. D.W.F. Brilman (Wim)
External Member: Prof.dr. G. Mul (Guido)

Acknowledgment

I am deeply grateful for the guidance and support provided by my supervisor, **Dr.ir. A.G.J van der Ham**. His motivation and continuous encouragement played a crucial role in the successful completion of this thesis.

I extend my gratitude to **Prof.dr. S.R.A. Kersten**, **Prof.dr.ir. D.W.F. Brilman**, and **Prof.dr. G. Mul** for their valuable inputs during the thesis midterm presentation.

I would like to acknowledge the immense sacrifices made by **my parents** and their unwavering support throughout my Master's journey, away from home. Their moral support and encouragement have been invaluable. A big thanks to my friends in Enschede, **Isabella, Preethi, and Julia**, who made these two years unforgettable. Lastly, I want to express my heartfelt gratitude to my boyfriend, **Ali**, for his constant encouragement, moral support, patience, and understanding.

Contents

1 Introduction **6**
- 1.1 Work Framing . . . 6
- 1.2 Objectives . . . 7
- 1.3 Chapters Organization . . . 7

2 State-of-art **9**
- 2.1 Overview of LOHCs . . . 9
  - 2.1.1 LOHCs Choice . . . 10
- 2.2 Overview of De-hydrogenation Process . . . 12
- 2.3 Overview of CO_2 Capture and Storage Methods . . . 14
- 2.4 Research Questions . . . 18

3 Results and Discussions **19**
- 3.1 Thermodynamic Analysis and Validation . . . 19
  - 3.1.1 MgO Carbonation . . . 19
  - 3.1.2 Methanol Steam Reforming (MSR) . . . 21
  - 3.1.3 MSR Coupled with In-situ CO_2 Capture by MgO Carbonation 27
- 3.2 Kinetic Analysis . . . 29
  - 3.2.1 MgO Carbonation . . . 29
  - 3.2.2 Methanol Steam Reforming (MSR) . . . 32
- 3.3 MSR with In-situ MgO Carbonation . . . 33
  - 3.3.1 Process Conditions . . . 34
  - 3.3.2 Post-Reaction Composition . . . 36

4 Process Design **42**
- 4.1 Block Flow Diagrams . . . 42
- 4.2 Post-MSR . . . 43
  - 4.2.1 WGS Post-Reaction . . . 46
  - 4.2.2 Possible Heat Integration . . . 47
  - 4.2.3 PSA and Combustion . . . 49
- 4.3 Process Flow Diagram: Flowsheet Analysis . . . 51

5 Conclusion **53**

6 Recommendations **54**

Appendix **59**

Glossary

A	Cross-sectional area	m^2
$c_{i,0}$	PSA impurity inlet concentration	mol/m^3
d_p	Particle diameter	mm
D	Column diameter	m
Ea	Activation energy	kJ/mol
ϵ	Solid occupancy in bed	$m^3{}_{solid}$/m3,reactor
ϵ_v	Bed voidage	$m^3{}_{void}/m^3{}_{reactor}$
$F_{MeOH,in}$	Methanol inlet flowrate	mol/s
f_m	Reynolds correction factor	-
k_0	Pre-exponential kinetic factor	1/s
k	Kinetic constant	1/s or 1/min
L	Column length or height	m
MW_i	Component molecular weight	g/mol or kg/kmol
ΔP_i	Partial pressure difference	bar or Pa
$P_{i,eq}$	Equilibrium partial pressure of i	bar
P_i	Partial pressure of i	bar
P_{ref}	Reference pressure	bar
r_i	Rate	kmol/(m^3·s) or kmol/(kg·s)
R	Ideal gas constant	J/(mol·K)
Re	Reynolds number	-
S	Conversion factor	-
S/C	Steam to carbon ratio	-
t*	Adsorption saturation time	seconds
u	Superficial gas velocity	m/s
mu	Gas mixture viscosity	Pa·s
Vreactor	Reactor volume	m^3
W/F	Catalyst mass to inlet flowrate ratio	kg·s/mol
$W_{sat,i}$	Saturation adsorbent capacity of i	-
x_{MgO}	MgO mass content in the promoted MgO	$kg_{MgO}/kg_{AMS-Mg_{95}Ca_5}$
ρ_i	Density of i	kg/m^3

List of Figures

Figure 1: LOHC Closed Loop Cycle. 8

Figure 2: Methanol to Hydrogen Conversion Routes [1]. 13
Figure 3: CO_2 Capture Methods Reported in Literature [2]. 15
Figure 4: CO_2 Mass Captured Using Different Methods Reported in Literature. 16
Figure 5: CO_2 Equilibrium Partial Pressure as a Function of Temperature for Different Metal Oxides [3]. 16
Figure 6: Alkali Metal Salt-Promoted MgO-$CaCO_3$ Sorbent [4]. . . . 18

Figure 7: RGIBBS Reactor Inputs and Outputs for Equation 6. . . . 20
Figure 8: P_{CO2} as a Function of Temperature of Equation 6 for Factsage, HSC Chemistry, and Aspen Plus. 20
Figure 9: Inputs and Outputs of the Aspen Model According to the Factsage Analysis. 21
Figure 10: Aspen Plus Model Vs. Factsage for $MgCO_3$ Steam Decomposition. 21
Figure 11: The Sensitivity Analysis of MgO Carbonation of Equation 6 at Total Pressure of 1 bar as a Function of Temperature. 22
Figure 12: Inputs and Outputs of the MSR Rgibbs Reactor. 22
Figure 13: Effect of Temperature and S/C on Methanol Conversion for Equation 3 for Inlet MeOH = 1 kmol/hr at 1 bar. 23
Figure 14: Effect of Temperature and S/C on Hydrogen Production for Inlet MeOH = 1 kmol/hr at 1 bar. 23
Figure 15: Effect of Temperature and S/C on CO and CO_2 Production for Inlet MeOH = 1 kmol/hr at 1 bar. A: S/C = 1, B: S/C = 1.5. 24
Figure 16: Effect of Temperature and S/C on Hydrogen Purity for Inlet MeOH = 1 kmol/hr at 1 bar. A: S/C = 1, B: S/C = 1.5. 25
Figure 17: Temperature Effect on Methanol Conversion at Different Pressures for Inlet MeOH = 1 kmol/hr and S/C = 1. . . . 25
Figure 18: Pressure Effect on Methanol Conversion and Partial Pressures of the Outlet Stream at 300 °C, Inlet MeOH = 1 kmol/hr, and S/C = 1. 26
Figure 19: Pressure and Temperature Effect on Methanol Conversion at Inlet MeOH = 1 kmol/hr, and S/C = 1. 26
Figure 20: Input-output Diagram of MSR In-situ and Off-situ CO_2 Carbonation by MgO. 28

Figure 21: Methanol Conversion as a Function of CO_2 Removal by MgO (In-situ vs. Off-situ) and Pressure at MeOH Inlet = 1 kmol/hr and S/C = 1. Where In-situ = CO_2 Produced:MgO = 1:1 and Off-situ = No MgO at Inlet. 29
Figure 22: Water Amount Formed as a Function of CO_2 Removal and Pressure at Inlet MeOH = 1 kmol/hr and S/C = 1. 30
Figure 23: Reactor Pressure and Temperature Effect on MgO Carbonation and Methanol Conversion in MSR at MeOH Inlet = 1 kmol/hr, S/C = 1, and MgO:MeOH = 1:1. 31
Figure 24: H_2 and CO_2 Pressures at 30 and 40 bar. 32
Figure 25: Effect of Pressure on CO_2 Conversion in MgO Carbonation for Inlet CO_2 = 357 kmol/hr at 300 °C and ϵ = 10%. 34
Figure 26: Effect of ϵ on CO_2 Conversion in MgO Carbonation for Inlet CO_2 = 357 kmol/hr at Total Pressure = 40 bar and 350 °C. 35
Figure 27: Effect of Temperature on CO_2 Conversion in MgO Carbonation for Inlet CO_2 = 357 kmol/hr at Total Pressure = 40 bar and ϵ = 5%. 36
Figure 28: The Base Case Used for Comparison Reasons in a MSR Coupled With In-Situ CO_2 Conversion by MgO. 37
Figure 29: Temperature Effect on CO Fraction and MeOH Conversion in the Combined MSR + MgO Kinetic Reactor. 38
Figure 30: MgO Presence Effect on CO Fraction in the Combined MSR + MgO Kinetic Reactor. 39
Figure 31: Adiabatic Reactor Effect on Methanol Conversion and CO Outlet Fraction in the Combined MSR + MgO Kinetic Reactor. 39
Figure 32: Effluent Temperature of the Adiabatic Reactor in the Combined MSR + MgO Kinetic Reactor. 40
Figure 33: Temperature Profile Across the Length of the Adiabatic Operated Reactor in the Combined MSR + MgO Kinetic Reactor. 40
Figure 34: Temperature Profile Across the Length of the Adiabatic Operated Reactor in the Combined MSR + MgO Kinetic Reactor. 41

Figure 35: BFD Scenarios. 42
Figure 36: CO Removal/Conversion Technologies [5, 6]. 43
Figure 37: Estimation (Based on Available Data) of the Compositions of Inlet and Outlet of the PSA Studied by Agueda et al. [7]. 44
Figure 38: BFD Updated Sequence. 45
Figure 39: Thermodynamic Analysis of Temperature Effect on WGS Post-MSR + MgO Carbonation Kinetic Reactor of the Base Case. 46
Figure 40: Kinetic Analysis of Temperature Effect on WGS Post-MSR + MgO Carbonation Kinetic Reactor of the Base Case. . . 47

Figure 41: A Rough Illustration of the WGSR Post-MSR + MgO Carbonation Kinetic Reactor Position. 48
Figure 42: First Scenario for Heat Integrating MSR Effluent with Inlet. 48
Figure 43: Second Scenario for Heat Integrating MSR Effluent with Inlet. 49
Figure 44: The Final Process Flow Diagram (PFD). 51

Figure 45: Experimental MgO Conversion Versus Time for Equation 6 Using AMS-$Mg_{95}Ca_5$ at 1 bar Total Pressure [4]. 60
Figure 46: Ln k Versus 1/T for MgO Carbonation after 5 Minutes. . . 62
Figure 47: MSR Kinetic Model Validation Using Methanol Conversion Versus Temperature for $m_{catalyst}$ = 1 kg and S/C = 1.5. . . 63
Figure 48: MSR Kinetic Model Validation for Pressure Effect Using Methanol Conversion Versus W/F at 39 bar and 533 K for $m_{catalyst}$ = 1 kg and S/C = 1. 63
Figure 49: MSR Kinetic Model Validation for Equilibrium Extents at 39 bar for $m_{catalyst}$ = 1 kg - 1000 kg and S/C = 1. 64

List of Tables

Table 1: Hydrogen Purity Requirements According to the ISO 14687-2. 8

Table 2: A Comparison of the Different Liquid Hydrogen Storage Systems [8, 9]. 11

Table 3: Methanol vs. Ammonia Properties for Hydrogen Storage [8, 9]. 12

Table 4: Decomposition Reaction Enthalpy for Metal Carbonates. . 17

Table 5: Summary of the MgO Carbonation Kinetic Parameters. . . 33

Table 6: Composition of the MSR + MgO Carbonation Reactor's Effluent at Base Case Conditions. 36

Table 7: Effect of WGS on CO Content Post-MSR + MgO Kinetic Reactor. 47

Table 8: Heat Integration Scenarios: Energy Requirement Comparison. 49

Table 9: The Compositions of the Hydrogen-saturated and Off-gas Leaving the PSA. 50

Table 10: Heaters and Coolers Inlet and Outlet Temperatures, and their Duties. 50

Table 11: Diameter and Length for PSA. 51

Table 12: Criteria Explanation for Hydrogen Storage Systems [9]. . . 59

Table 13: Physical Properties of Different Components 60

Table 14: AMS-$Mg_{95}Ca_5$ Skeletal and Bulk Density Calculations from Composition and Data by Cui et al. [4]. 61

Table 15: MgO Carbonation Reaction Kinetic Constant After 5 Minutes. 61

Table 16: Saturation Time for CO_2 and CO. 65

Table 17: Properties of PSA Feed Mixture: Obtained from Aspen Plus. 65

1. Introduction

1.1 Work Framing

The extensive utilization of fossil fuels has a profound impact on the escalation of Greenhouse Gas (GHG) levels in the atmosphere [10]. As public awareness regarding the environmental consequences of fossil fuels grows, there is an increasing interest in seeking cleaner alternative options for fuel and energy. This poses a significant challenge as we strive to meet the rising energy demands resulting from population growth while simultaneously aiming at reducing our carbon footprint. In 2016, the Paris Agreement [11] established targets for nations to pursue, aiming for renewable and green energy resources to account for a significant portion of the world's primary energy requirements.

Hydrogen is a very promising candidate for replacing fossil fuel used for many applications in the energy sector as it has the highest energy per mass of fuel while forming only water when it reacts. When compared with gasoline, hydrogen has a much higher gravimetric energy density (120 MJ/kg vs. 44 MJ/kg) [8]. Hydrogen, if produced by renewable means such as wind or solar energy, can be a great substitute to fossil fuels. It produces water and releases energy when reacted with oxygen or air, making it a water forming molecule and eco-friendly. However, the main drawback of hydrogen is the challenge of storing it efficiently due to its very low volumetric energy density of 3 Wh/L under ambient conditions [8], which is more than 3200 times less than that of gasoline. Pressurizing hydrogen between 200 - 700 bar can increase the volumetric energy density to a range between 0.5 up to 1.5 kWh/L while liquid hydrogen could store 2.3 kWh/L. Up until today, several storage technologies have been proposed, i.e. physical storage systems. This method requires high pressure or very low temperature for proper storage due to hydrogen having very low boiling temperature (around 20 K). Also, both of these systems require enormous amounts of energy to compress or liquefy hydrogen. For example, liquefying 1 kg of hydrogen will cost 36% of the energy contained in the same amount of hydrogen [12]. In addition, special materials that should handle such harsh conditions throughout the journey are needed to control the amount of hydrogen losses that could result from boil offs [9].

As a result, various storage technologies, other than physical methods, have been suggested such as Liquid Organic Hydrogen Carriers (LOHCs) [9], metal hydrides [9], ammonia [8], and methanol [8, 9, 13]. Methanol is now considered a competitive hydrogen storage system when compared with the other possible alternatives for hydrogen storage systems. That is due to its high theoretical hydrogen gravimetric capacity (ranging from 12.1 wt.% in case of methanol decomposition to CO [9] up to 18.75 wt.%[1]), its low cost, availability, ease of transport and storage due to its boiling point of 65 °C, and its industrially mature reversibility for hydrogen release. The most concerning disadvantage of methanol is its toxicity of handling, and CO/CO_2 generation during thermal decomposition or reforming [8, 9].

[1] When methanol is steam reformed according to $CH_3OH + H_2O \leftrightarrow CO_2 + 3\,H_2$

Research have been focusing on ways to capture CO_2 efficiently as the conventional benchmark for this separation process, absorption by amine solutions, is not convenient in terms of capture capacity, reversibility, and energy demand. Currently, metal oxides such as CaO and MgO are being explored as a method to capture and store CO_2 at medium temperature operations (200 °C - 500 °C) [2].

The thesis framework focuses on investigating methanol as a liquid hydrogen carrier compared to other liquid options currently available in the market. Since methanol produces CO_2 during the reforming process to produce H_2, it is essential to implement CO_2 capture techniques. In this regard, the suitability of MgO is studied as a potential candidate for CO_2 capture during methanol steam reforming.

1.2 Objectives

The project will focus on hydrogen release from methanol (as seen in the right-hand side, or the de-hydrogenation, of Figure 1) in the Netherlands to be used in a Polymer Electrolyte Membrane (PEM) fuel cell according to the ISO 14687-2. The main objectives of this project is to:

- Compare methanol with the other storage systems available in the market/under research in a literature review and study the use of methanol as a hydrogen carrier.
- Study the carbon capture and storage methods for long-term transportation of CO_2.
- Analyze the process for hydrogen production from methanol in combination with CO_2 capture using MgO.
- Ensure the purity of hydrogen meets the requirements set by the fuel cells as seen in Table 1.
- Methanol is fed at 100 ktonne/year and methanol conversion of $\geq$99% is required.
- Process design: the study is done using Aspen Plus flowsheet simulator and no experimental work is included.

1.3 Chapters Organization

The thesis report is split to 5 main chapters:

- **Chapter 1: Introduction** | includes work framing, objectives, and chapters organization.
- **Chapter 2: State-of-art** | provides a literature review and overview of different LOHCs, de-hydrogenation techniques, and CO_2 capture methods.

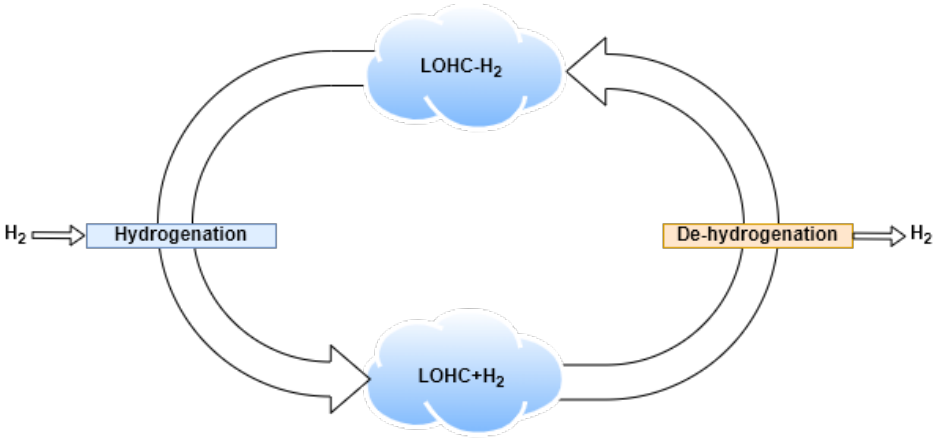

Figure 1: LOHC Closed Loop Cycle.

Table 1: Hydrogen Purity Requirements According to the ISO 14687-2.

Characteristics	**Mole fraction (%)**
Hydrogen	99.97
Maximum Allowable Contaminants Concentration (μmol/mol)	
Water	5
Total hydrocarbons	2
Carbon dioxide	2
Carbon monoxide	0.2

- **Chapter 3: Results and Discussions** | here, the results from the simulations done are analyzed and discussed.
- **Chapter 4: Process Design** | in this section, the Block Flow Diagrams (BFDs) and Process Flow Diagram (PFD) are discussed.
- **Chapter 5: Conclusions** | summarizes the project outcomes and answers the research questions.
- **Chapter 6: Recommendations** | gives suggestions and recommendations for future work depending on the challenges faced.

2. State-of-art

2.1 Overview of LOHCs

According to the objectives listed in Chapter 1.3, the distance of which hydrogen will travel is considered a long-distance transportation. Hydrogen molecule exists as gas at atmospheric conditions and as a liquid at 20 K. Compressed (CGH_2) at pressures $>$ 200 bar and liquefied hydrogen (LH_2) transportation are the most used storage options [9, 14]. In CGH_2 systems, high electricity demand is needed to compress hydrogen, especially for mobile storage. On the other hand, applications show that liquefying hydrogen needs more than 35% of the energy that the stored hydrogen actually contains. In addition, 1 - 5% per day of the stored hydrogen boils off when using liquefied storage system which results in loss of volume. Moreover, both, CGH_2 and LH_2 systems, impose high safety requirements due to high pressures or very low temperatures [9].

Due to these reasons, alternatives to physical storage systems are now being researched such as storage in solid and liquid forms. Solid systems could either be a result of physiosorption or chemisorption of hydrogen on solids [15]. Physiosorbed hydrogen on solids like activated carbon show advantageous results in terms of reversibility and kinetics. However, they tend to need very low temperatures for proper loading of hydrogen. For example, at 25 °C, hydrogen loading do not exceed 5 wt.% [16]. On the other side, metal hydrides involve the chemisorption of hydrogen on metal solids to produce hydrides. The latter showed high hydrogen density (around 10 wt.%), however, their hydrogenation, de-hydrogenation, and reversibility are tough and complex [17]. As a result, solid-state systems will no further be considered.

LOHCs are another method to store hydrogen, but in liquid form. They are considered a cheap and an easily manageable method for long-term energy storage without boil-offs and losses. For efficient hydrogen storage using LOHCs, a closed cycle involving the hydrogenation of LOHC at the hydrogen source and the de-hydrogenation for hydrogen release at the destination of hydrogen usage should be implemented. LOHCs impose a huge advantage in terms of long distance transportation due to their similarities to crude oil properties making it easy to use the same ships or trucks for transportation [9].

Ammonia possesses high hydrogen density (17.7 wt.%) and deems to be suitable for long-term transportation applications. It is not considered as a LOHC because its main constituents forming it completely split after de-hydrogenation as seen in Equation 1.

$$2NH_3 \rightarrow N_2 + 3H_2 \tag{1}$$

The main disadvantage of ammonia is its high energy requirement for de-hydrogenation being around 15 MJ/kg-H_2 which is equivalent to 12.5% of the energy stored in 1 kg of hydrogen. In addition, the effluents need a proper separation to provide a high purity, nitrogen-free hydrogen stream [8].

Methanol is a competitive molecule, especially to ammonia, to store and transport hydrogen [8]. As mentioned earlier, care should be taken when handling methanol due to its toxicity and flammability. In addition, the de-hydrogenation process, via steam reforming, involves CO_2 production [9]. As a result, CO_2 separation and storage is important. However, depending on the separation technology, the process might deem to be energy intensive. For instance, using the conventional amine solution absorption systems for CO_2 capture requires at least 174 kJ/mol-CO_2 or 3.96 MJ/kg-CO_2 [18]. This means that for 1 kg H_2 produced, which is equivalent to 7.3 kg of CO_2 using Methanol Steam Reforming (MSR) route, 24% of hydrogen's energy content (120 MJ/kg-H_2) is used for CO_2 capture. When comparing this value with the energy duty needed for the methanol de-hydrogenation through steam reforming (49.7 kJ/mol-MeOH or 1.6 MJ/kg-MeOH), it can be seen that CO_2 capture using amine consumes 3.5 times more energy than that needed for the main reforming reaction. As a result, to use methanol as a hydrogen carrier, efficient CO_2 capture and storage method should be implemented.

Although the main objective is to study methanol as a potential hydrogen carrier, it should also fit the objectives of the project. Therefore, a comparison should be made between LOHCs, ammonia, and methanol.

2.1.1 LOHCs Choice

Storing hydrogen in LOHCs, methanol, or ammonia is currently used for long-term or long distance hydrogen transportation as they store hydrogen in the form of liquid. The main characteristics to look for when comparing these systems are: capacity, reversibility, safety, availability, energy demand, etc [9]. Moreover, as hydrogen will travel a long distance, the volumetric hydrogen content (kg-H_2/m^3) or energy density (kWh/L) plays an important role in screening possible methods for this application [8]. Table 12 in the Appendix explains the frame conditions and criteria of selection in a more detailed manner. It is to be noted that heat integration between hydrogenation and de-hydrogenation is not possible when the two processes are happening at different locations.

A lot of LOHCs are studied in the literature, but only few of them are further considered in the comparison. The latter are: N-ethylcarbazole (NEC) , dibenzyltoluene (DBT), formic acid (FA), napthalene (NAP), toluene (TOL), and phenazine (PHE). In addition to these, methanol (METH), which is considered a circular carrier, and ammonia (NH3) are also added as very competitive hydrogen storage methods and will be considered in the next chapters.

Table 2 shows a good comparison between these different liquids for hydrogen storage. It is important to point out the most important frame conditions for the proposed process. For a long-term transportation system, a liquid with a high energy density is needed to make sure more energy is stored within the same volume in a ship. Compared to gasoline, which has an energy density of 8.9 kWh/L, methanol exhibits significant competitive potential as a hydrogen carrier,

especially considering that the energy density of hydrogen as a liquid does not surpass 2.3 kWh/L. From this perspective, it is seen that methanol and ammonia show the highest possible hydrogen contents and energy densities. In addition to that, they are produced globally on large scales, so these compounds are relatively cheap and available. Moreover, Methanol Steam Reforming (MSR) and ammonia thermal-chemical decomposition as the de-hydrogenation processes of methanol and ammonia are technologically mature according to the technological readiness level (TRL)[1] which is 9 and 4 - 7, respectively [9, 19, 20]. It can be noted though that methanol steam reforming is a much mature process when compared with ammonia decomposition. Nevertheless, methanol steam reforming energy demand is the lowest looking at all other storage systems in Table 2 with a value of 16.5 kJ/mol-H_2. This is almost half of what is required by ammonia thermal decomposition.

Table 2: A Comparison of the Different Liquid Hydrogen Storage Systems [8, 9].

Frame Conditions	**NEC**	**DBT**	**FA**	**NAP**	**TOL**	**PHE**	**METH**	**NH3**
Gravimetric hydrogen content (wt.%)	5.2 - 5.8	6.2	0.3 - 4.4	7.4	5.9 - 6.2	2.4 - 7.2	12.5 - 18.75[2]	17.64[3]
Energy density (kWh/L)	2.5 - 2.25	1.9	0.1 - 1.8	2.2	1.5 - 1.6	0.8 - 2.4	3.3 - 4.95[2]	3.52
Global production	Limited	Large	Limited	Large	Large	Limited	Large	Large
Price (€/kg)	40	4	30	0.6	0.3	26	0.5	1
Toxicity	Toxic	Low	Low	Toxic	Toxic	Toxic	Toxic	Toxic
De-hydrogenation temperature	180 - 270	310	100	280	250 - 450	190	100 - 400	400
De-hydrogenation Energy (kJ/mol-H_2)	53.2	65.4	31.2	66.3	68.3	61.3	16.5	30
Liquid at ambient conditions	No	Yes	Yes	No	Yes	No	Yes	Yes
TRL	3	9	3	4	8	3	9[4]	4 - 7[5]

In many literature studies, it was seen that ammonia shows higher gravimetric and volumetric hydrogen content than methanol. That is due to these literature assuming that hydrogen released from methanol follows the methanol decomposition reaction to CO. However, it can be assumed that methanol can undergo the steam reforming reaction which then produces 3 hydrogen molecules instead of 2 in the decomposition route. As a result, the theoretical hydrogen content is much

[1]The TRL is a method to assess how developed a technology is in the industry.
[2]Hydrogen weight % based on 3H2 with respect to 1 mol of methanol
[3]Hydrogen weight % based on 3H2 with respect to 2 moles of ammonia
[4]TRL based on high temperature steam methanol reforming
[5]TRL of power-to-NH_3 via Haber-Bosch and thermal-chemical decomposition of NH_3 to H_2

higher than what is usually reported in the literature, 18.8 wt.% versus 12.1 wt.% [8, 9]. Table 3 shows a comparison between methanol and ammonia according to a hydrogen energy density of 120 MJ/kg, and methanol decomposition in presence of steam.

Table 3: Methanol vs. Ammonia Properties for Hydrogen Storage [8, 9].

Properties	**Methanol**	**Ammonia**
Gravimetric hydrogen content (wt.%)	18.8	17.6
Density (kg/m^3) at 25 °C, 1 and 10 bar, resp.	792	600
Volumetric hydrogen content (kg-H_2/m^3)	149	106
Energy density (MJ/kg)	22.5	22

Although ammonia has the advantage of no direct CO_2 emissions unlike methanol, rather it produces N_2. Also, ammonia needs to be pressurized for transport while methanol does not. Moreover, the hydrogen release process for methanol happens at much lower temperatures than ammonia decomposition (>200 °C versus >400 °C, respectively).

In summary of this comparison, methanol (through steam reforming) emerges as a compelling candidate for hydrogen storage in long-distance transportation, particularly when contrasted with other researched or commercially employed organic liquids. Notably, in comparison to ammonia, which demands pressurization for storage, methanol does not need external energy to stay in a liquid state under storage conditions. The subsequent task entails selecting an appropriate dehydrogenation method for methanol to release the hydrogen for utilization in a fuel cell.

2.2 Overview of De-hydrogenation Process

Methanol at the arrival to Rotterdam can be de-hydrogenated to hydrogen through different routes as illustrated in Figure 2.

Methanol Decomposition (MD) follows the reaction in Equation 2 which involves only methanol as the reactant. It is a catalytic reaction that occurs at temperatures >400 K. However, it is dismissed due to high catalyst poisoning from the formation of CO and less hydrogen production compared to the other routes [1].

$$CH_3OH \leftrightarrow CO + 2H_2 \qquad \Delta H^{\circ}_{\text{rxn}} = +90.7\,\text{kJ/mol} \tag{2}$$

Methanol Steam Reforming (MSR) provides high conversion of methanol and large yields of hydrogen due to involvement of steam next to methanol. It produces

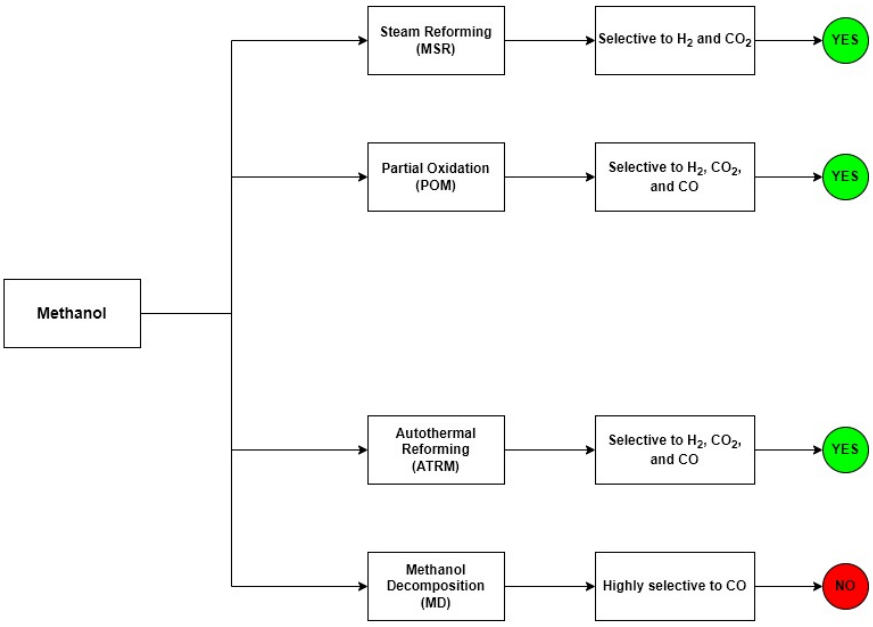

Figure 2: Methanol to Hydrogen Conversion Routes [1].

insignificant amount of CO, so it is more selective towards CO_2. MSR is an endothermic reaction at a reaction enthalpy of 50 kJ/mol-Methanol according to Equation 3. It is possible to occur at temperatures >200 °C, but might need higher temperatures due to kinetic limitations. In addition, MSR is a very mature process and the technology is industrially widely applied with a TRL of 9 [9, 1].

$$CH_3OH + H_2O \leftrightarrow CO_2 + 3H_2 \qquad \Delta H^\circ_{\text{rxn}} = +49.7\,\text{kJ/mol} \tag{3}$$

On the other hand, Partial Oxidation (POM) is an exothermic reaction that occurs by reacting air or oxygen with methanol at temperatures between 30 °C - 450 °C. The combustion requires oxygen below the stoichiometry as seen in Equation 4 to control the combustion products. For this reason, the syngas produced is rich in CO. Moreover, it usually has half the selectivity the MSR has for H_2 [1]. For this reason, more purification could be needed before the fuel cell. As a result, this process is dismissed.

$$CH_3OH + 0.5O_2 \leftrightarrow CO_2 + 2H_2 \qquad \Delta H^\circ_{\text{rxn}} = -192\,\text{kJ/mol} \tag{4}$$

Autothermal Reforming (ATRM) reaction in Equation 5 is a thermal neutral process. Although ATRM offers higher efficiency and conversions than POM, it still produces high amount of CO and requires a lot of purification ahead of the PEM. This process shows higher H_2 yields than POM. However, the catalyst is complex and a post-purification step is needed to remove CO [1].

$$CH_3OH + (1-2r)H_2O + rO_2 \leftrightarrow CO_2 + (3-2r)H_2 \quad (5)$$

Where r is the ratio of oxygen to methanol at the inlet.
To conclude, the MSR seems to provide simplicity of operation, maturity in industrial applications, low CO selectivity, and high conversion of methanol. Consequently, it is the de-hydrogenation method that will be implemented in the next stage.

2.3 Overview of CO_2 Capture and Storage Methods

As MSR follows the reaction in Equation 3, it can be seen that to provide a pure hydrogen stream, CO_2 or H_2 should either be removed as they form. Also, this removal will help in prohibiting the products from the water gas shift reaction (WGS) which will reduce the hydrogen content and increase CO fraction at the outlet.

Nowadays, membrane reactors (Pd - Ag) are studied to separate H_2 as it is formed [1]. This way, the equilibrium is shifted towards the products side leading to higher conversions at lower temperatures. However, these membranes are expensive and highly sensitive to ppms of CO which forms during MSR due to the methanol decomposition as a side reaction [9, 21].

In this project, the focus will be on removing CO_2 as it is being formed instead of separating H_2 in a membrane. CO_2 production is a big drawback to methanol being a hydrogen carrier. Therefore, a comparison on the available CO_2 capture methods is needed.

Figure 3 shows a good comparison between the reported methods to capture and store CO_2. Amine-based absorption systems is the most conventional and mature process in industry where MEA is currently used in large scales for CO_2 capture [2]. In addition to the fact that the highest reported CO_2 capacity of amine-based solvents do not exceed 44 g-CO_2/kg-solvent, this process is also energy intensive due to high energy requirement in the solvent regeneration step [22]. Also, amines are corrosive [23], making storage, transportation, and handling a critical aspect of using it.

On the other hand, adsorption offers an advantage of reusing the adsorbent a lot of times. However, the adsorbents in the market do not show high capacities towards CO_2 [24]. For example, activated carbon (AC) can handle up to 88 g-CO_2/kg-AC as a maximum, which is a relatively small number.

Besides amine-based solvents being a conventional process to capture CO_2, liquefaction of CO_2 is also a mature process for CO_2 storage and transport. The main disadvantage of this process is that the conditions at which CO_2 could be stored is around -55 °C at 20-40 bar. This means that the storage tanks should be

pressurized and refrigerated during the shipping process.

Finally, chemical looping, which involves carbonation of metal oxides to form metal carbonates in the form of solids. These solids should have high capacity towards CO_2 at MSR conditions, and require acceptable temperature ranges for the decomposition of the metal carbonate to release CO_2 again. As a result, the solid should also handle high temperatures and do not degrade with cycles, this is why, it is named as "looping" [2, 25, 26, 3].

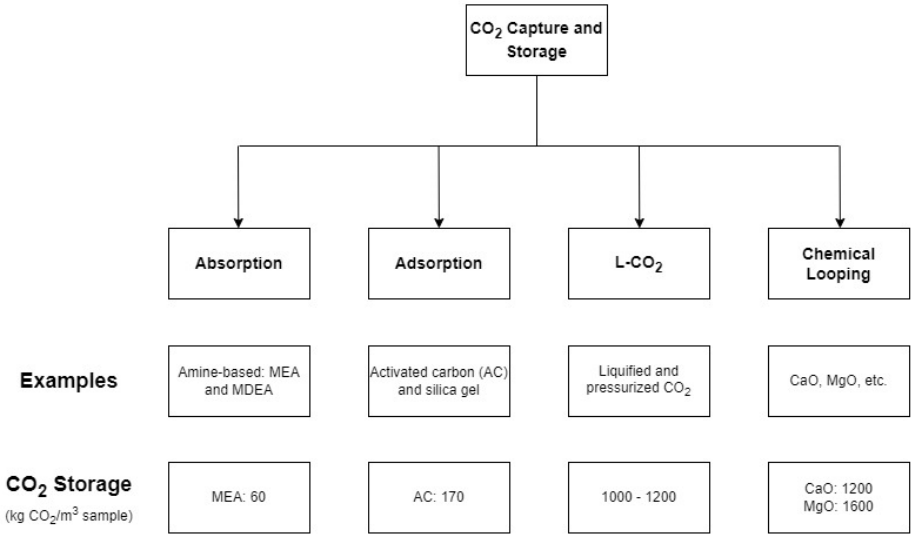

Figure 3: CO_2 Capture Methods Reported in Literature [2].

When talking about long-distance shipping, then storage volume is very important. For a 1 m^3 space, Figure 4 shows a visual comparison of how much mass of CO_2 can be stored using various storage samples at ideal conditions (and using skeletal densities). It is therefore concluded that chemical looping using metal oxides is the process to proceed with for CO_2 capture and storage in this project.

The most studied metal oxide in literature is CaO due to its availability. Other metals that could be promising are magnesium, lithium, barium, sodium, and potassium. The higher the basicity of their oxides, the harder it is to decompose the metal carbonate. So, the carbonation of LiO_2, Na_2O, K_2O, and BaO are irreversible due to their very high basicity [3]. Figure 5 shows a comparison between metal oxides available on the basis of their equilibrium CO_2 partial pressure of carbonation as a function of temperature. The curve stops for some compounds due to their melting point. At the same CO_2 partial pressure, it is seen that MgO carbonation could start at a much lower temperature compared to the other metal oxides in Figure 5. In a Methanol Steam Reforming (MSR) reaction operating at pressures >20 bar and temperatures above 280 °C for full conversions of methanol, a CO_2 partial pressure of 5 - 10 bar is expected to be at the effluent. As a result, MgO can be a good candidate theoretically for CO_2 capture due to its suitability

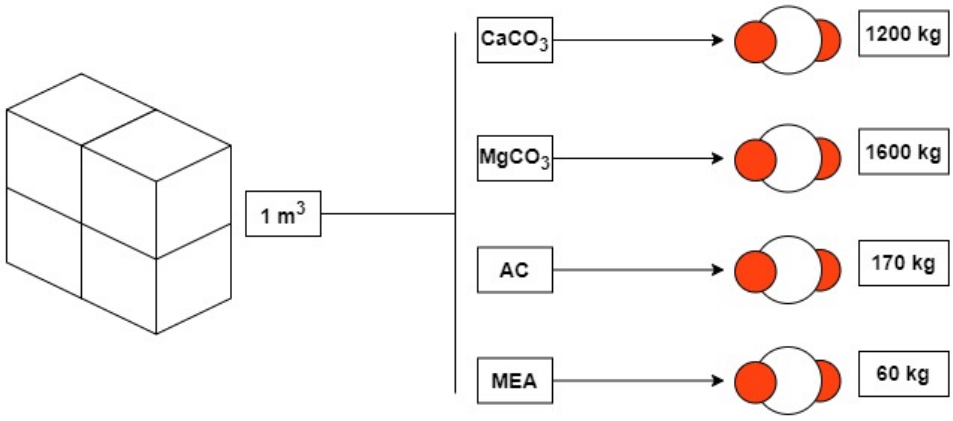

Figure 4: CO_2 Mass Captured Using Different Methods Reported in Literature.

for the operating regime in typical applications of an MSR [3] as seen in the blue shaded area in Figure 5. In addition, magnesium-based oxides are available in huge amounts and are considerably cheap [25].

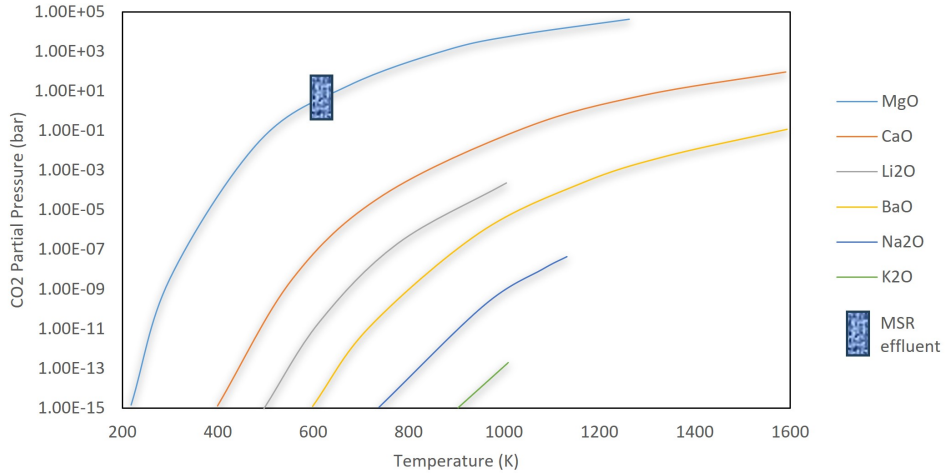

Figure 5: CO_2 Equilibrium Partial Pressure as a Function of Temperature for Different Metal Oxides [3].

To make a good choice, one should also consider the decomposition or the reverse reaction. This is because the captured CO_2 should be released at the hydrogen source to produce methanol again. As a result, it is wise to look at the decomposition reaction enthalpies for the different metal carbonates compared in Figure 5. Table 4 illustrates in numbers that it is less energy intensive to decompose $MgCO_3$ than any other metal carbonate. Theoretically, this also means that the temperature needed for this reaction can be much lower than that required for the other carbonates. In real life applications, this is not always true.

Pure MgO carbonation is kinetically a very slow process even at higher tempera-

Table 4: Decomposition Reaction Enthalpy for Metal Carbonates.

Metal Carbonate	ΔH°_{rxn} **(kJ/mol)**
$MgCO_3$	118
$CaCO_3$	178
Li2CO_3	226
$BaCO_3$	226

tures and pressures [27, 28]. As a result, some research focused on enhancing the performance of MgO by adding promotors, increasing its surface area, or changing the synthesis method. A.-T Vu et al. [29] prepared Na_2CO_3 - $NaNO_3$ doped MgO using supercritical drying procedure. The solid was able to reach 50% of the theoretical CO_2 capacity at 325 °C and 1 bar. A better performance was seen in a study by Y. Qiao et al. [30] preparing $NaNO_3$ - $NaNO_2$ - doped MgO by impregnation method. The results reached 80% of the theoretical capacity at 350 °C and 1 bar.

Although the previous work seems promising, having high CO_2 capacity is not enough, as it is important to look at the rate at which these values are reached. The previous experiments were performed for over 2 hours, which makes the process very slow overall. A recent comparison done by G. Ji et al [28] in 2020 for CO_2 sorption rates in magnesium-based sorbents shows that the rate can be increased up to 0.13 g-CO_2/(g·min) when using a pure CO_2 stream at 1 bar [4]. Alkali-metal salts (AMS) such as $LiNO_3$, KNO_3, Na_2CO_3, and K_2CO_3 are used to increase the CO_2 capacity of pure MgO to a maximum of 0.25 g-CO_2/g-sorbent in 5 mins which is around 22% of the maximum capacity. To maintain a high cyclic stability, H. Cui et al [4] proposes an AMS-prompted MgO-$CaCO_3$ sorbent which can achieve up to 60% of the theoretical CO_2 capacity in 5 mins at 350 °C and 1 bar of CO_2 partial pressure. The promoted sorbent used by Cui et al. [4] is seen in Figure 6.

Another important factor that can increase MgO carbonation rate is the addition of steam. Experimental work shows that commercial MgO carbonation with pure CO_2 stream at 20 bar and 300 °C is kinetically much slower (almost no conversion of MgO) to when compared with a stream of CO_2 mixed with 5 vol% steam in the inlet at the same pressure where full conversion is seen for the same time given for both setups. This is due to $MgCO_3$ forming a layer around MgO and prohibiting any further CO_2 mass transfer to MgO to occur. As a result, fine particles of MgO are suggested as it can result in a fast and full conversion at mild operating conditions. The authors state that high CO_2 pressure is needed next to steam to achieve $> 90\%$ conversion of MgO to $MgCO_3$, yet it is not well studied [31]. In this work, the effect of steam on the rate of MgO carbonation will not be considered.

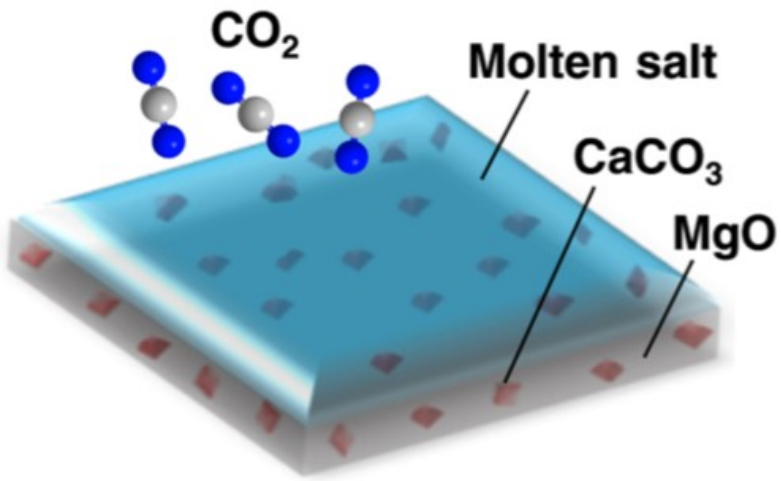

Figure 6: Alkali Metal Salt-Promoted MgO-$CaCO_3$ Sorbent [4].

As a conclusion, the AMS-MgO-$CaCO_3$ sorbent will be used in this process. Initially, a thermodynamic analysis on MgO carbonation will be done and then the kinetic model presented by H. Cui et al [4] will be implemented in Aspen Plus next to the MSR.

2.4 Research Questions

After the literature review, the research questions that can be answered in the thesis project are:

- To what extent can MgO help in capturing CO_2 during the Methanol Steam Reforming (MSR)?
- What are the conditions under which MSR can operate in a way that fits the objectives of the project?
- What is the outlet composition of a kinetic reactor that involves MSR and MgO carbonation at the chosen conditions?
- What are the post-reaction units needed to achieve the required hydrogen purity for the fuel cell?
- Can MgO carbonation supply enough energy for the MSR when happening simultaneously?
- What is the extra energy needed to have a full process from hydrogen production to producing a $\geq 99.97\%$ hydrogen pure stream?

3. Results and Discussions

3.1 Thermodynamic Analysis and Validation

3.1.1 MgO Carbonation

For the thermodynamic analysis, the Aspen Plus software is used by employing the "Rgibbs" reactor which analyzes the thermodynamic properties of the different components to give the equilibrium state of the input reactants. The process will include two main reactions: methanol steam reforming (MSR), and magnesium oxide carbonation. The MSR reaction is a very mature process, and the thermodynamic properties associated with its forming reactants are well known in literature and will not be validated. On the other hand, magnesium-based thermodynamic properties are not reliable as they differ from one source to another. As a result, literature suggests further experimental work for determining the operating window for magnesium-based carbonates [27]. This section will discuss the validity of the available thermodynamic data in Aspen Plus compared to the most reliable experimental work done on MgO carbonation reaction.

The MgO carbonation follows Equation 6. This reaction is exothermic and is favored at lower temperatures. To analyze this reaction in Aspen Plus, the property package chosen is "SOLIDS". MgO and $MgCO_3$ properties vary from one reference to another in literature and different property packages show varying results for the decomposition temperature of $MgCO_3$ as seen in Figure 7 [27, 32].

$$MgO + CO_2 \rightarrow MgCO_3 \qquad \Delta H^{\circ}_{\text{rxn}} = -118\,\text{kJ/mol} \tag{6}$$

For this reason, a number of programs used in literature will be addressed and compared to experimental results validating the conditions at which $MgCO_3$ is formed. These thermodynamic property packages are used in the programs Factsage, HSC Chemistry, and Aspen Plus. CO_2 partial pressure can be plotted as a function of temperature for the three different programs. In Figure 7, the three former software are plotted. Experimental work show that $MgCO_3$ can be formed at P_{CO2} of 0.5 bar at 373 °C or at P_{CO2} of 0.78 bar at 385 °C [33, 27, 31].

The Aspen Plus model included the inputs and outputs according to Figure 7.

In Figure 8, it is clear that Factsage package shows a much better illustration of the real data for MgO carbonation to $MgCO_3$. Donat et al. [27] state in their work that Factsage program represent well the experimental results in literature for the same reaction, which is not the case looking at HSC Chemistry database.

From this perspective, it is wise to compare the results of Aspen Plus for MgO carbonation with that of Factsage. Stating that Aspen Plus can imitate the Factsage thermodynamic performance for this reaction means that the model is validated with experimental work as Factsage results is close to that of the experimental

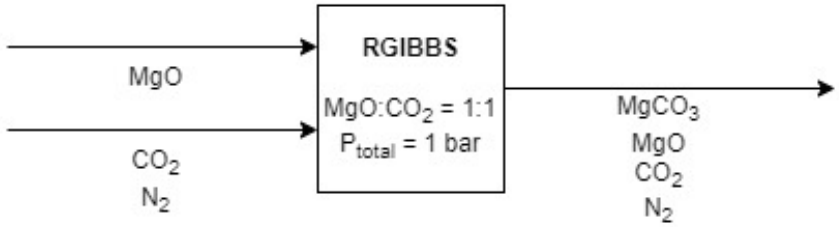

Figure 7: RGIBBS Reactor Inputs and Outputs for Equation 6.

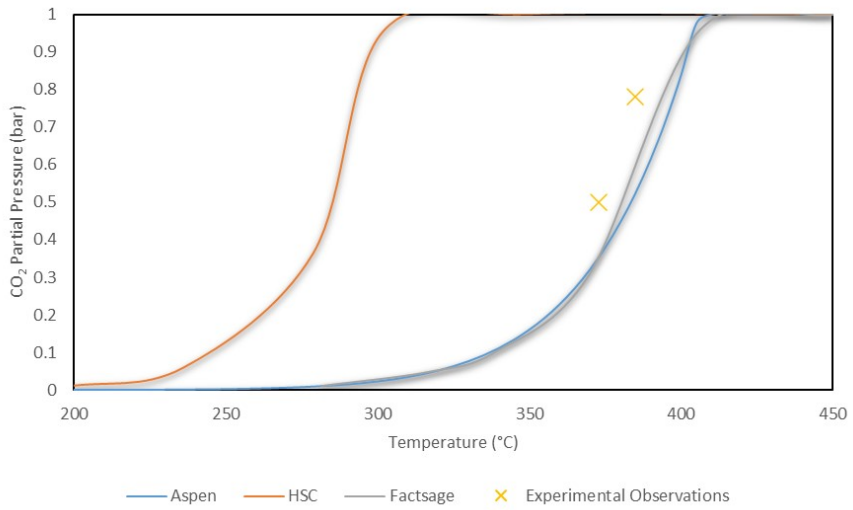

Figure 8: P_{CO2} as a Function of Temperature of Equation 6 for Factsage, HSC Chemistry, and Aspen Plus.

observation.

In this way, the Aspen Plus model can be used in the next stage as it is validated with Factsage. In addition to that, Ranjani et al. [32] did a thermodynamic study on $MgCO_3$ formation and decomposition. Using the same Aspen model, the results will be compared with the latter study [32] at a total pressure of 1 bar, 0.1 moles of N_2, and 1 mole of H_2O according to Figure 9.

The comparison shows that the Aspen model produces the same results seen from Factsage as presented in Figure 10. After the validation, the optimum operating conditions for the MgO carbonation reaction can be studied. To do this, a sensitivity analysis is done on the system as a function of temperature as shown in Figure 7. To capture CO_2 as it is produced from the MSR, enough partial pressure of CO_2 should be available at the reactor temperature. In the analysis seen in Figure 11, at low temperatures, P_{CO2} is very low, which illustrates that all CO_2 present from methanol conversion is already converted to $MgCO_3$. This is also explained by the exothermicity of the reaction as seen in Equation 6. Low reactor temperature is thermodynamically favored towards $MgCO_3$ formation, although kinetically limited. The final temperature choice will depend largely on the MSR operating conditions and the carbonation temperature of MgO to $MgCO_3$.

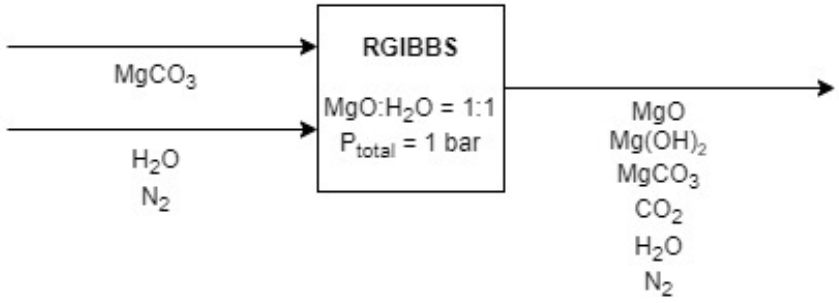

Figure 9: Inputs and Outputs of the Aspen Model According to the Factsage Analysis.

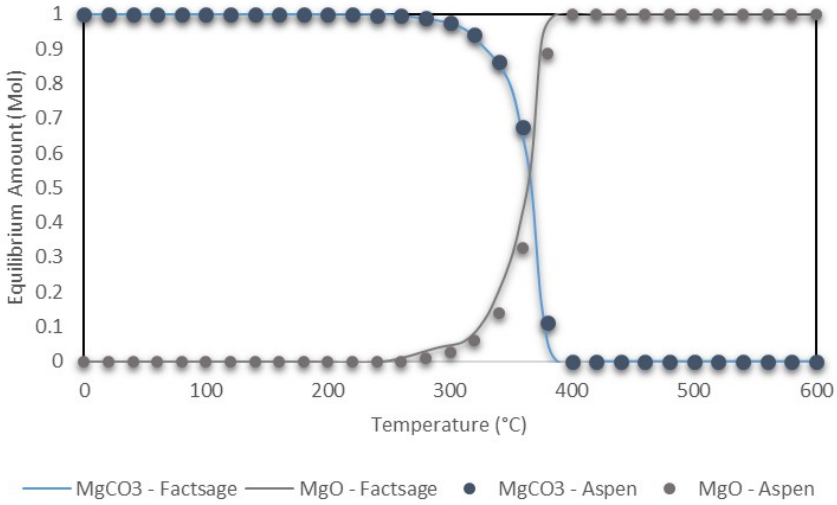

Figure 10: Aspen Plus Model Vs. Factsage for $MgCO_3$ Steam Decomposition.

3.1.2 Methanol Steam Reforming (MSR)

To produce hydrogen from methanol, steam reforming is the most industrially mature technology for this conversion [9]. This is done via the MSR (Equation 3), Methanol Decomposition (Equation 7), and Reverse Water Gas Shift (Equation 8).

$$CH_3OH \leftrightarrow CO + 2H_2 \tag{7}$$

$$CO_2 + H_2 \leftrightarrow CO + H_2O \tag{8}$$

To choose the optimum operating conditions of the MSR, the steam to carbon ratio (S/C), pressure, and temperature, are all important factors to consider. In addition to this, the components to be included in the thermodynamic analysis on Aspen Plus RGIBBS outlet is crucial. The most common components seen in literature are: CH_3OH, H_2O, CO, CO_2, H_2, CH_4, and C [34]. However, formation of methane and carbon are a function of the catalyst used. For instance, Ni-based catalysts would catalyze the products to undesired products such as carbon. In

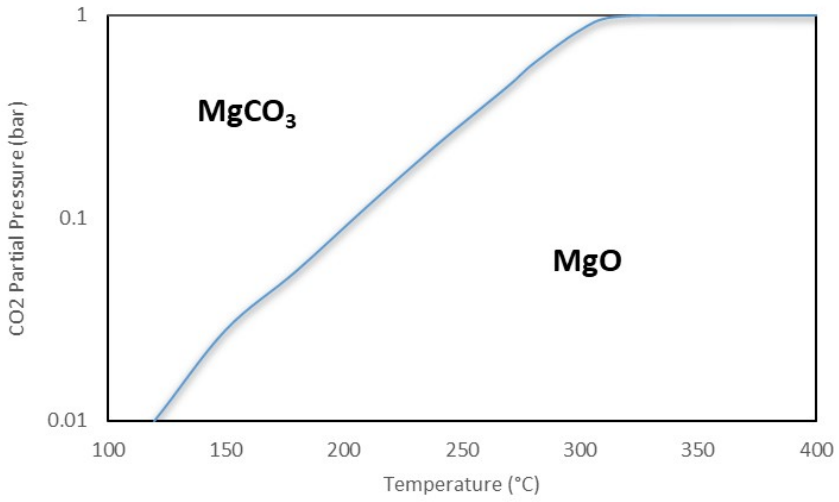

Figure 11: The Sensitivity Analysis of MgO Carbonation of Equation 6 at Total Pressure of 1 bar as a Function of Temperature.

this project, Ni-based catalysts will not be used. Therefore, it is assumed that the formation of methane and carbon in the Rgibbs can be neglected.

Steam to Methanol Ratio

Initially, the methanol conversion as a function of temperature is studied for different S/C mol ratios in the inlet for the system shown in Figure 12. The amount of steam fed into the system is represented by "x" which is controlled by the S/C ratio.

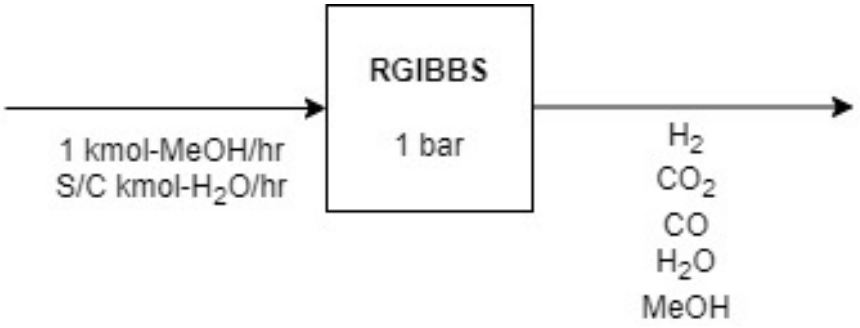

Figure 12: Inputs and Outputs of the MSR Rgibbs Reactor.

The analysis is represented in Figure 13 at 1 bar total pressure. It can be seen that the higher the S/C, the higher is the conversion of methanol at all temperatures, although the difference is not really significant above 250 °C. This is mainly due to the shift of the reaction towards the right side in order to decrease the amount of steam added in the reactants' side of the equilibrium.

A higher steam flowrate would lead to more hydrogen being produced in the effluent as illustrated in Figure 14. The maximum hydrogen production seen is around

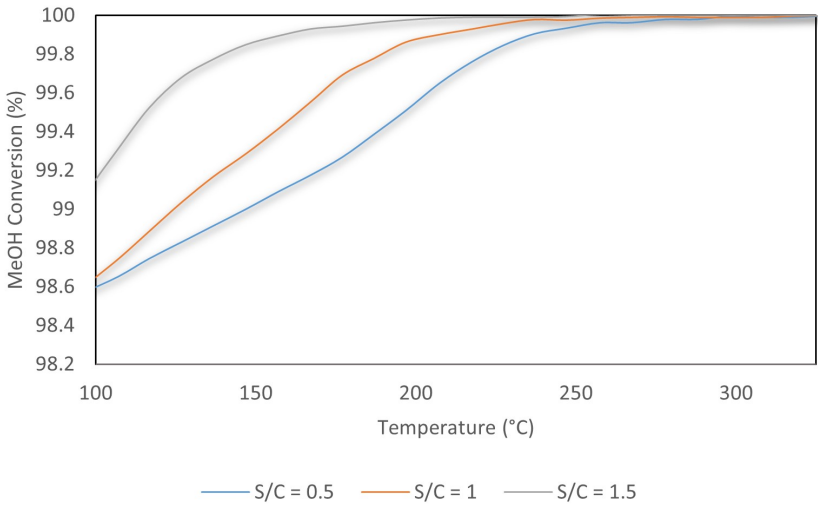

Figure 13: Effect of Temperature and S/C on Methanol Conversion for Equation 3 for Inlet MeOH = 1 kmol/hr at 1 bar.

3 kmol/hr at S/C = 1.5. In this figure, it is also seen that as the temperature increases above 180 °C, hydrogen is being consumed due to the RWGS seen in Equation 8. For this reason, the S/C choice should be high enough that reaction 8 is more favorable towards CO_2, yet ensuring not a lot of steam is left over as this will require more separation post-reaction. Also, more steam in the feed requires extra energy to evaporate up to reactor conditions. In addition, the catalyst used can be negatively affected by excess steam.

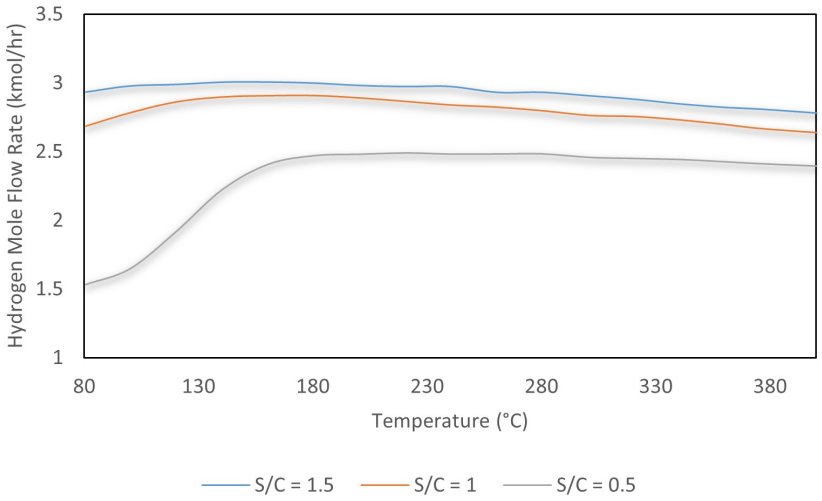

Figure 14: Effect of Temperature and S/C on Hydrogen Production for Inlet MeOH = 1 kmol/hr at 1 bar.

Figure 15 shows how for S/C of 1 and 1.5, the flow rates of CO and CO_2 changes minimally. In addition, the CO_2/CO ratio is seen to be larger for higher S/C due to more CO_2 produced at S/C = 1.5 as discussed earlier. However, as temperature

increases, the fraction decreases to a very low value due to the RWGS reaction. Yet, the difference is not significant.

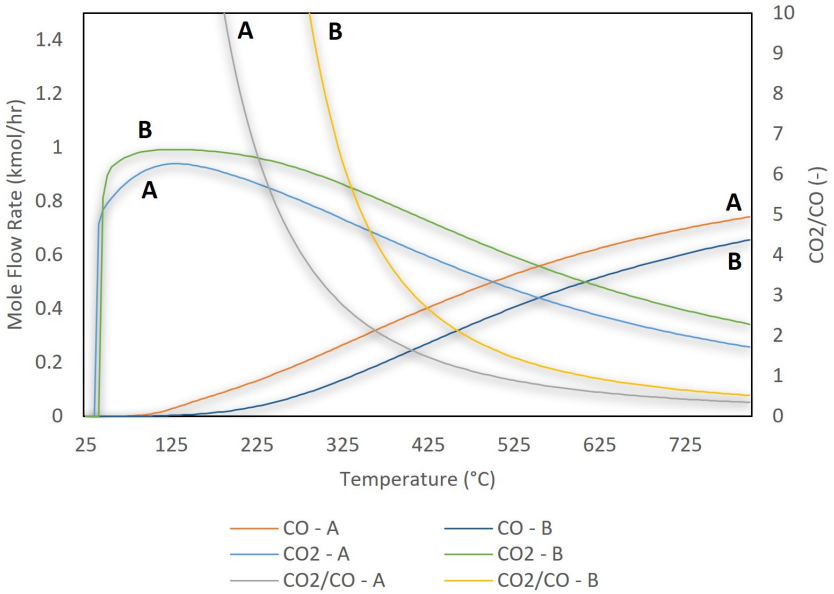

Figure 15: Effect of Temperature and S/C on CO and CO_2 Production for Inlet MeOH = 1 kmol/hr at 1 bar.
A: S/C = 1, B: S/C = 1.5.

A drawback of having excess steam in the feed is that the fraction of hydrogen produced will be lower as it is shown in Figure 16. This will require more post-treatment after the reactor which is undesirable. As a result, a S/C of 1 is chosen and will be used in the next sections.

Temperature and Pressure Effect

It was shown in previous figures that as temperature rises, the conversion is higher due to the endothermicity of the reaction. However, the optimum choice will largely depend on the combination of the MSR and MgO carbonation reactions. For now, the temperature should be >200 °C for MeOH conversions $\geq$ 99%. Especially when the pressure is increased much more above 1 bar, and when kinetics are included, higher temperatures would be needed for full conversions.

As methanol is fully converted at temperatures >200 °C, the pressure effect will only be seen at lower temperatures as shown in Figure 17. Although high pressures can decrease the methanol conversion according to Le Chatelier's principle, it is industrially more favored to operate at high pressures up to 40 bar. This is because pressurizing methanol and water is less costly than having to pressurize hydrogen at the outlet for transportation or short-term storage. In Figure 19, it can be seen that pressures above 20 bar can reduce MeOH conversion significantly. On the other hand, Using a 100% efficient compressor will still require around 5% of the hydrogen's energy content to compress it from 20 bar to 500 bar

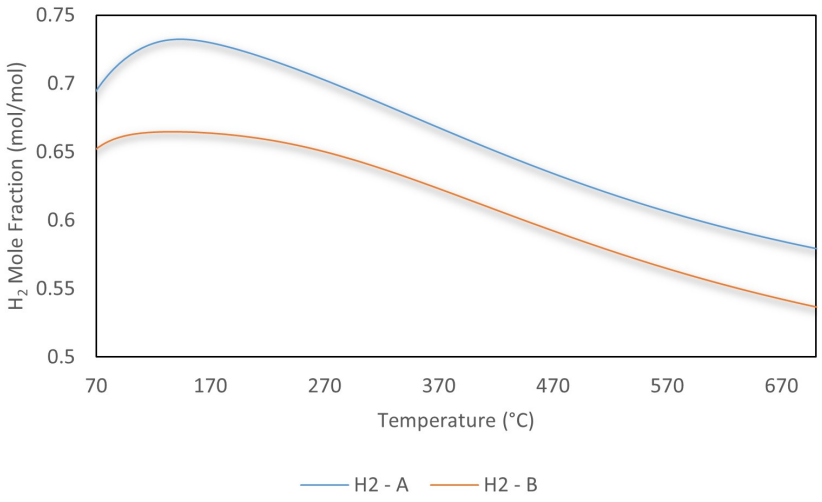

Figure 16: Effect of Temperature and S/C on Hydrogen Purity for Inlet MeOH = 1 kmol/hr at 1 bar.
A: S/C = 1, B: S/C = 1.5.

[35]. This obviously means that it will always be beneficial to operate the MSR at high pressures to generate hydrogen at higher partial pressures on the expense of lower MeOH conversions. The lower the compressor's inlet pressure is (lower MSR reactor pressure), the more energy intensive hydrogen compression becomes. Moreover, the higher the MSR pressure is, the higher the partial pressure of CO_2, which will result in higher driving force for MgO carbonation.

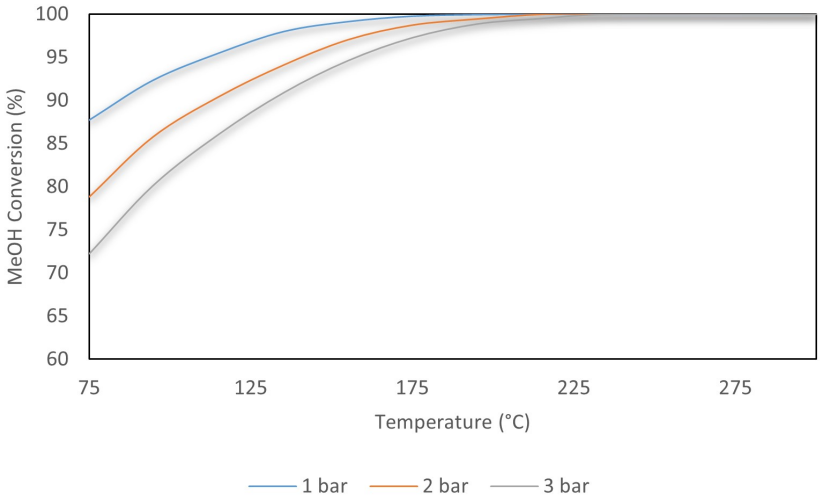

Figure 17: Temperature Effect on Methanol Conversion at Different Pressures for Inlet MeOH = 1 kmol/hr and S/C = 1.

An analysis for pressures between 1 - 40 bar is done on the MSR reactor at 300 °C. It can be stated from Figure 18 that methanol conversion can drop from 100% to 95% by increasing pressure to 40 bar. On the other hand, as stated earlier, Figure

18 shows that, although the conversion is dropping, the increase in the pressure will lead to producing higher partial pressures of CO_2 and H_2. As a result, the compression costs of hydrogen will be lower. In addition to that, CO_2 carbonation to $MgCO_3$ will be faster for higher CO_2 pressures.

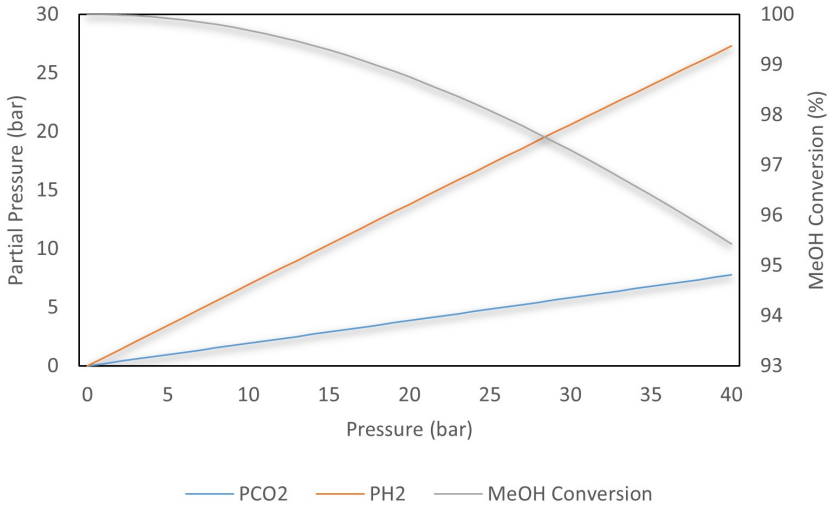

Figure 18: Pressure Effect on Methanol Conversion and Partial Pressures of the Outlet Stream at 300 °C, Inlet MeOH = 1 kmol/hr, and S/C = 1.

For now, looking at Figure 19 which zooms on a pressure window of 20 - 40 bar, it can be concluded that for a higher pressure process, a higher temperature is needed to reach a certain conversion.

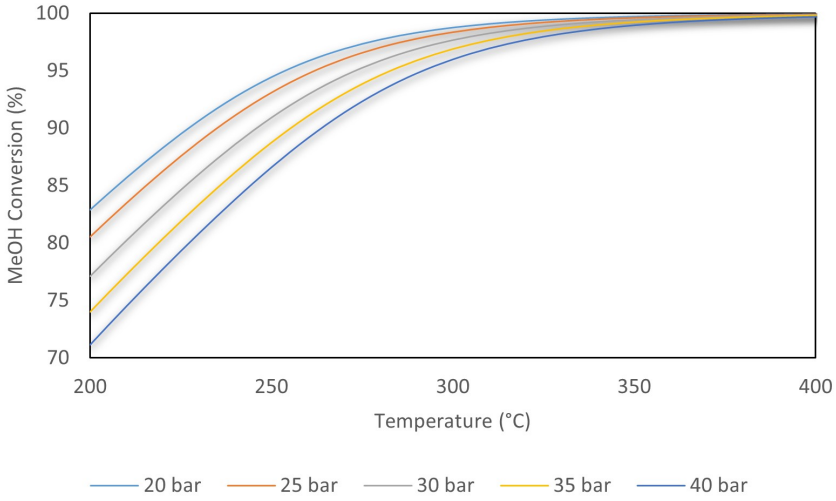

Figure 19: Pressure and Temperature Effect on Methanol Conversion at Inlet MeOH = 1 kmol/hr, and S/C = 1.

From the individual analysis, the conditions at which the MSR and MgO carbonation are thermodynamically favored are known. However, it is important to

ensure what components can be formed thermodynamically, and what conditions fit best the combination of both reactions in-situ. This is needed for the kinetic rate analysis.

Methane and Carbon Formation

Methane and carbon are possible products to be formed during the MSR. If that is the case, it is important to know at what conditions they form as these products are undesirable because it reduces the selectivity towards the desired products, CO_2 and H_2. In addition, carbon can deactivate the catalyst and block the reaction from proceeding.

From the thermodynamic analysis, which included carbon and methane next to MeOH, H_2O, H_2, CO, CO_2, it was seen that methane is a possible product to be formed at 1 bar of reaction between temperatures of 300 °C - 400 °C while carbon can form at lower temperatures.

To control the formation of these products, the catalyst chosen should not contain any Nickel in its composition. Nickel-based catalysts favor the formation of methane from MSR. Cu-based catalysts can be used to avoid the formation of carbon. As a result, a $Cu/ZnO/Al_2O_3$ catalyst is chosen for the MSR as it is the commercial catalyst and it avoids the formation of the undesired products.

3.1.3 MSR Coupled with In-situ CO_2 Capture by MgO Carbonation

The final choice for pressure and temperature can be made after adding MgO to the inlet of the reactor. This is because CO_2 is removed as it is formed, shifting the reaction towards higher conversions at the same temperature. As of now, the S/C is concluded that it should be ≥ 1 (off-situ) to favor the steam reforming reaction over methanol decomposition towards CO. The temperature window will depend on the final choice of pressure, kinetics, and the optimum MgO carbonation conditions.

In-situ Vs. Off-situ CO_2 Capture

In-situ CO_2 removal from MSR has many benefits when compared with off-situ process. These include:

- Reduces the shift towards the RWGS reaction seen in Equation 7.
- CO_2 removal shifts the MSR equilibrium towards the products side.
- Less water production from the RWGS as water has a lot of side effects on the Cu-based catalysts for MSR.
- One reactor is needed instead of two reactors, although more complex.

According to the input-output diagram in Figure 20, at 20 - 40 bar, and a temperature range of 200 °C - 500 °C, the methanol conversion is plotted in Figure 21. It can be seen that conversions in in-situ process is $> 99\%$ for the full temperature range where the off-situ showed full conversions only at temperatures $\geq 400\,^{\circ}C$ presented in Figure 21(d).

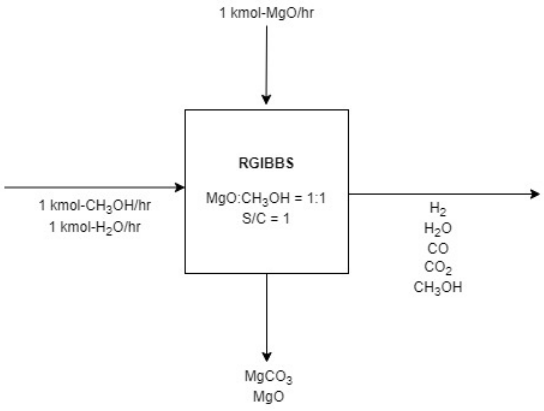

(a) In-situ

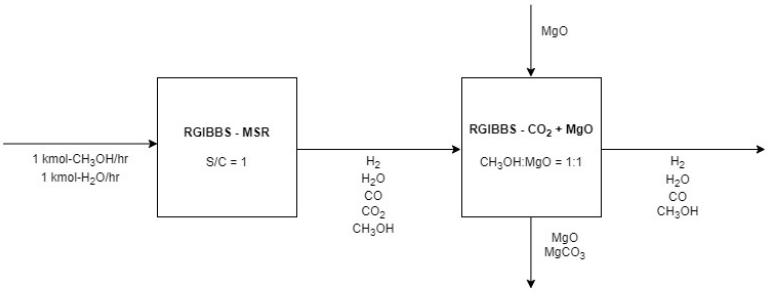

(b) Off-situ

Figure 20: Input-output Diagram of MSR In-situ and Off-situ CO_2 Carbonation by MgO.

Additionally, Figure 22 shows that in-situ capture can largely reduce water production from RWGS in Equation 8 when compared with off-situ process. This is seen because during in-situ CO_2 removal, the reaction of RWGS in Equation 8 is not favored. The reduction ranges between 5 - 100 % absolute values below the temperature at which full methanol conversion is reached as a function of operating pressure.

Temperature and Pressure Effect

As it was discussed, a higher pressure will reduce the methanol conversion, but increase the outlet CO_2 partial pressure which then leads to an increased capture capacity for MgO according to the MgO carbonation reaction in Equation 6. Figure 23(a) shows the MgO conversion as a function of temperature and pressure. A higher reactor pressure will show higher MgO conversions at lower temperatures.

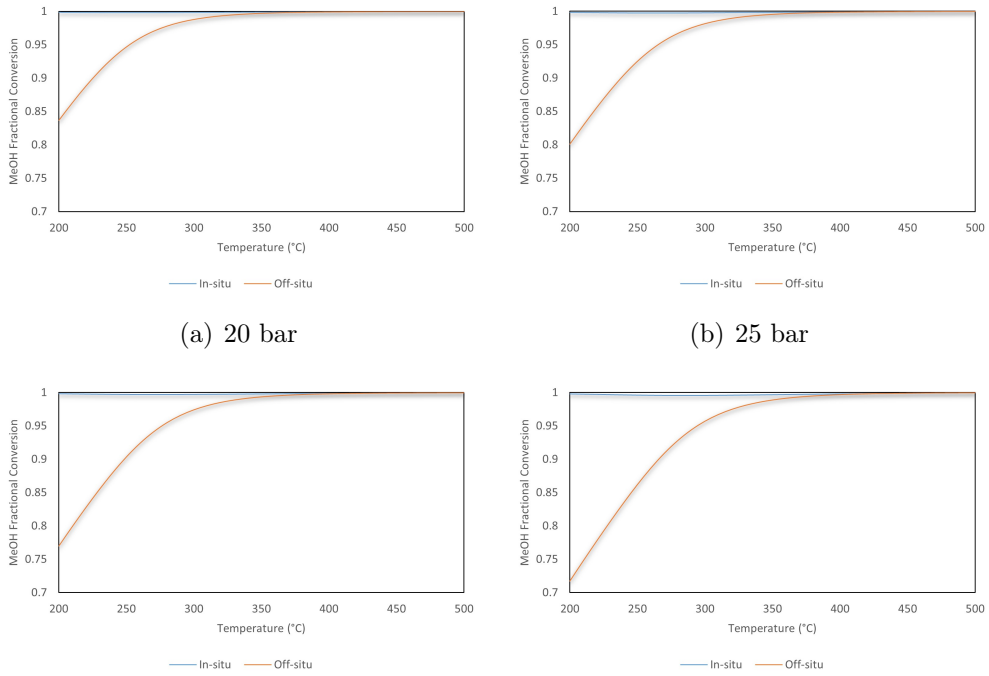

(a) 20 bar

(b) 25 bar

(c) 30 bar

(d) 40 bar

Figure 21: Methanol Conversion as a Function of CO_2 Removal by MgO (In-situ vs. Off-situ) and Pressure at MeOH Inlet = 1 kmol/hr and S/C = 1.
Where In-situ = CO_2 Produced:MgO = 1:1 and Off-situ = No MgO at Inlet.

Figure 23(b) shows the methanol conversion for in-situ CO_2 removal. The high temperature shows higher MeOH conversions indeed. As a result, choosing the temperature should be high enough for methanol conversion, and low enough for MgO carbonation. In addition, the kinetics is favored at higher temperatures, so it is always a good idea to operate at high temperatures. For this reason, a temperature of 350 °C seems to be the most suitable at pressures $>$ 30 bar, balancing high enough methanol and MgO conversions.

To choose the operating pressure, it can be seen that the difference of conversions at 30 bar and 40 bar is insignificant. Thus, the pressures of H_2 and CO_2 can judge by seeing Figure 24. The difference is significant in terms of hydrogen pressures (close to operating pressure). As a result, an operating pressure of 40 bar will be chosen to ensure a high partial pressure of hydrogen at the effluent.

3.2 Kinetic Analysis

3.2.1 MgO Carbonation

Kinetic Model

The kinetic model used is deduced from the data of the conversion of MgO as a function of time published by H. Cui et al. [4]. As it is desired to have a relatively

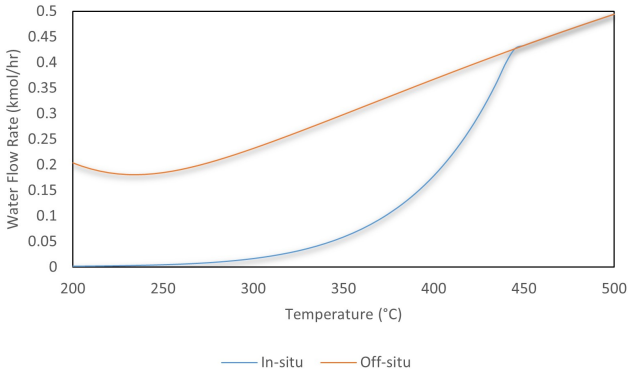

(a) 20 bar

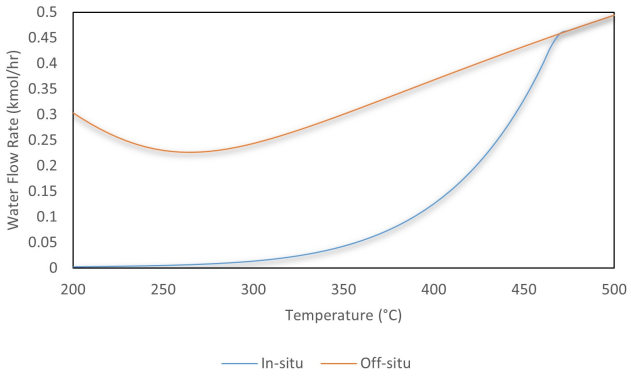

(b) 40 bar

Figure 22: Water Amount Formed as a Function of CO_2 Removal and Pressure at Inlet MeOH = 1 kmol/hr and S/C = 1.

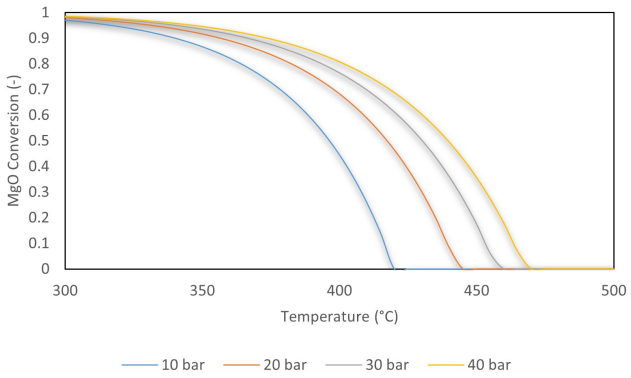

(a) MgO Conversion

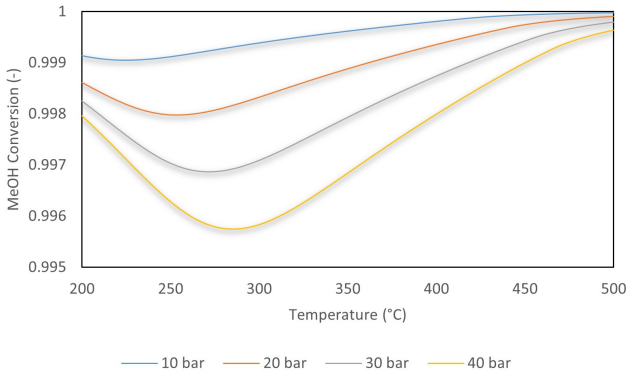

(b) Methanol Conversion

Figure 23: Reactor Pressure and Temperature Effect on MgO Carbonation and Methanol Conversion in MSR at MeOH Inlet = 1 kmol/hr, S/C = 1, and MgO:MeOH = 1:1.

fast conversion, the rate equation is obtained from the straight line relation after 5 minutes of the reaction as seen from Figure 45. This is a conservative estimate of the rate and it is explained in details in the Appendix.

As a conclusion to this section, Table 5 summarizes the kinetic model equation used in Aspen Plus alongside the values of each parameter. According to the model validation in the Appendix, MgO excess of 40% will be used to control the kinetics as per what is listed in the paper published by Cui et al. [4].

Sensitivity Analysis

MSR is favored at low pressures, however, MgO carbonation reaction rate increases with higher pressures as can be seen in Equation 12. Figure 25 shows that with increasing total pressure from 1 bar to 40 bar, the reactor volume decreases significantly (by a factor of $\tilde{1}6$).

According to Equation 12, the S factor includes ϵ, ρ_{MgO}, and x_{MgO}. The latter two are constants, while e can vary depending on the design. Figure 26 shows

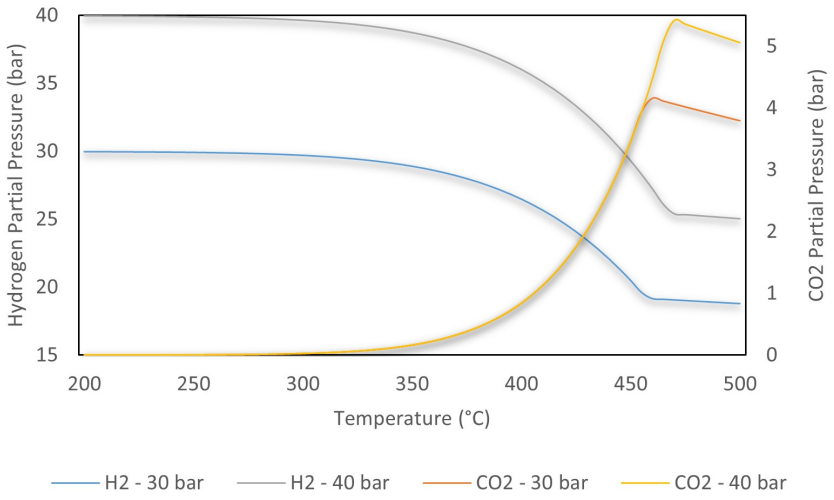

Figure 24: H_2 and CO_2 Pressures at 30 and 40 bar.

the effect of ϵ on the volume of reactor needed for CO_2 conversion in an MgO carbonation reactor using pure CO_2. As ϵ increases from 5% to 10%, the reactor volume needed to reach the same conversion decreases linearly.

As opposed to thermodynamics for MgO carbonation, as temperature increases from 300 °C to 400 °C, the volume needed decreases as seen in Figure 27. This effect is seen because the reaction becomes faster, decreasing the volume needed to reach a certain conversion.

3.2.2 Methanol Steam Reforming (MSR)

Kinetic Model

The model used to describe the kinetics of MSR on $Cu/ZnO/Al_2O_3$ catalyst is from Peppley et al. [36]. MSR occurs next to two other reactions, Equations 7 and 8. The model equations are described in Equations 9, 10, and 11 for MSR, MD, and Water Gas Shift Reaction (WGSR), respectively. Details on parameters estimation and detailed expressions are available in the publication [36].

$$r_{MSR} = \frac{k_{MSR} K^*_{CH_3O^{(1)}} (\frac{p_{CH_3OH}}{p^{0.5}_{H_2}}) (1 - (\frac{p^3_{H_2} p_{CO_2}}{k_{MSR} p_{CH_3OH} p_{H_2O}})) C^T_{S_1} C^T_{S_{1a}}}{(1 + K^*_{CH_3O^{(1)}} (\frac{p_{CH_3OH}}{p^{0.5}_{H_2}}) + K^*_{HCOO^{(1)}} p_{CO_2} p^{0.5}_{H_2} + K^*_{OH^{(1)}} (\frac{p_{H_2O}}{p^{0.5}_{H_2}}) + K_{CO^{(1)}_2} p_{CO_2}) (1 + K^{0.5}_{H^{(1a)}} p^{0.5}_{H_2})} \tag{9}$$

$$r_{MD} = \frac{k_{MD} K^*_{CH_3O^{(2)}} (\frac{p_{CH_3OH}}{p^{0.5}_{H_2}}) (1 - (\frac{p^2_{H_2} p_{CO}}{k_{MD} p_{CH_3OH}})) C^T_{S_2} C^T_{S_{2a}}}{(1 + K^*_{CH_3O^{(2)}} (\frac{p_{CH_3OH}}{p^{0.5}_{H_2}}) + K^*_{HCOO^{(2)}} p_{CO_2} p^{0.5}_{H_2} + K^*_{OH^{(2)}} (\frac{p_{H_2O}}{p^{0.5}_{H_2}}) + K_{CO^{(2)}_2} p_{CO_2}) (1 + K^{0.5}_{H^{(2a)}} p^{0.5}_{H_2})} \tag{10}$$

Table 5: Summary of the MgO Carbonation Kinetic Parameters.

$\mathbf{rCO_2} = \frac{k_0 \cdot e^{\frac{-Ea}{RT}} \cdot (\frac{P_{CO2} - P_{CO2,eq}}{P_{ref}}) \cdot x_{MgO} \cdot \rho_{MgO} \cdot \epsilon}{100 \cdot MW_{MgO}}$	
k_0 (seconds^{-1})	71
Ea (kJ·mol^{-1})	28
R (kJ·mol^{-1}·K^{-1})	8.3×10^{-3}
$P_{CO2,eq}$ (bar)	$\frac{1}{e^{\frac{T}{13636} - 20.01}}$
x_{MgO} (kg_{MgO}·kg$^{-1}{}_{AMS-Mg_{95}Ca_5}$)	0.657
ρ_{MgO} (kg·m^{-3})	1907
ϵ ($m^3{}_{MgO}$·m$^{-3}{}_{reactor}$)	0.05
MW_{MgO} (kg·kmol^{-1})	40

$$r_W = \frac{k_W^* K_{OH^{(1)}}^* (\frac{p_{CO} p_{H_2O}}{p_{H_2}^{0.5}})(1 - (\frac{p_{H_2} p_{CO_2}}{k_W p_{CO} p_{H_2O}}))C_{S_1}^{T^2}}{(1 + K_{CH_3O^{(1)}}^* (\frac{p_{CH_3OH}}{p_{H_2}^{0.5}}) + K_{HCOO^{(1)}}^* p_{CO_2} p_{H_2}^{0.5} + K_{OH^{(1)}}^* (\frac{p_{H_2O}}{p_{H_2}^{0.5}}) + K_{CO_2^{(1)}} p_{CO_2})^2} \tag{11}$$

The model validation can be found in the Appendix. In this project, the catalyst density is set to 1300 kg/m^3 and $\epsilon = 60\%$.

3.3 MSR with In-situ MgO Carbonation

After validating both kinetic models for MSR and MgO carbonation (See Appendix), one combined reactor can be used to proceed with modeling an MSR reactor with in-situ CO_2 removal by MgO. A base case in Figure 28 is identified first where one or more parameters' effect are studied. W/F used in this base case is fixed to 82 kg·s·mol^{-1} to ensure high enough conversions, even though this value is considered quite high for industrial applications due to the need for huge amount of catalyst. This value of W/F is equivalent to a reactor volume of 10.5 m^3 for a feed of 357 kmol-MeOH/hr (or 100 k-tonnes-MeOH/year). To calculate the corresponding reactor volume needed for a certain methanol flowrate at W/F, check the Appendix.

The outlet composition of the base case condition reactor is seen in Table 6.

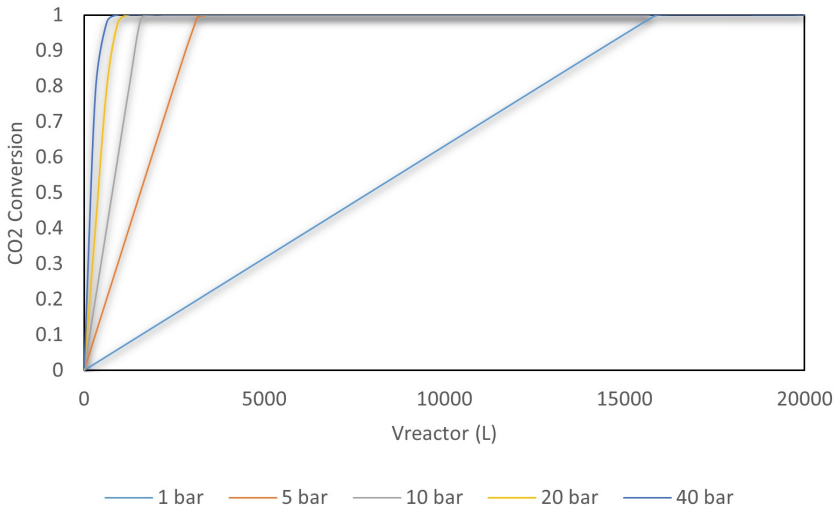

Figure 25: Effect of Pressure on CO_2 Conversion in MgO Carbonation for Inlet CO_2 = 357 kmol/hr at 300 °C and ϵ = 10%.

3.3.1 Process Conditions

In this reactor, several process conditions affect the final choice of the pre and post-reaction process units. The main conditions to analyze in such a reactor are: temperature, S/C, MgO inlet amount (if any), and reactor thermal configuration.

Temperature Effect

Almost full methanol conversion (∼98%) is seen at 350 °C and 40 bar at the conditions given in the base case, when isothermal operation is considered. MeOH conversion goes up to 99.7% in an adiabatic operated reactor. However, CO level in the effluent is a very important aspect to consider due to the high limitation put for fuel cell applications (maximum 0.2 ppm of CO allowable). Figure 29(a) and Figure 29(b) shows the temperature effect on CO level in the outlet stream, and methanol conversion, respectively.

It is seen that a higher temperature produces more CO across the bed due to the favoring of the WGS which converts CO_2 to CO, but it increases the methanol conversion. At an inlet temperature of 300 °C, 99% methanol conversion is reported in the adiabatic reactor. However, at the same inlet temperature, around 6% of CO exist in the effluent. As a result, to limit the CO fraction in the outlet stream, temperature should be controlled.

S/C Effect

Another way of limiting CO fraction in the effluent is by increasing the S/C ratio which favors the MSR towards CO_2. However, this means that more steam is left in excess which requires extensive water removal post-reaction. More details on this effect will be discussed in Chapter 3.3.2 to study the effect on heater duty alongside CO levels.

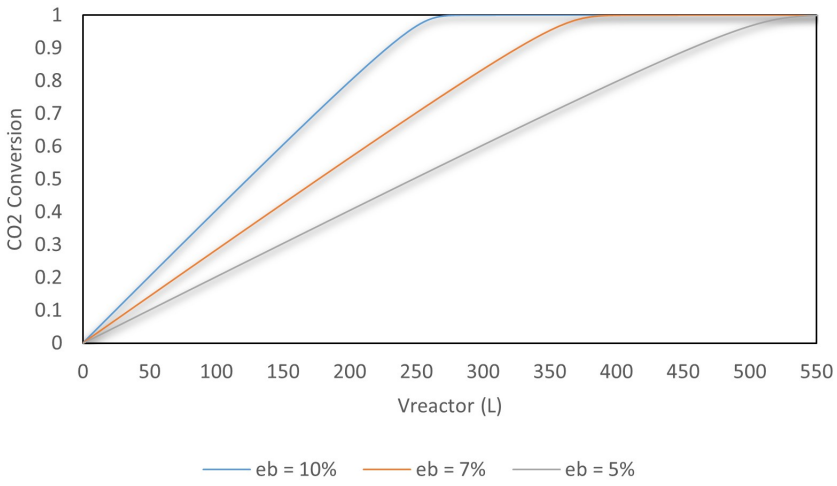

Figure 26: Effect of ϵ on CO_2 Conversion in MgO Carbonation for Inlet CO_2 = 357 kmol/hr at Total Pressure = 40 bar and 350 °C.

MgO Presence

Presence of MgO allows for high in-situ removal of CO_2. In the base case conditions, 93% conversion of CO_2 is seen towards $MgCO_3$. The CO_2 carbonation by MgO does not only affect CO_2 levels, it also reduces significantly the CO fraction in the outlet as the WGS reaction is prohibited due to CO_2 removal. This can be seen in Figure 30.

Adiabatic Reactor

In real life applications, reactors act adiabatic if no thermal control is taking place, such as continuous cooling/heating during the reaction. All figures shown previously where plotted at isothermal conditions according to the base case. Figure 31(a) shows the effect of an adiabatic operated reactor on methanol conversion. Inlet temperature does not have a big effect on methanol conversion because even for a lower inlet temperature, the increase in temperature due to CO_2 carbonation increases the methanol conversion. On the other hand, Figure 31(b) shows that a higher inlet temperature results in a higher CO fraction in the outlet.

For both temperature inlets, the outlet temperature of the effluent does not exceed 405 °C as seen in Figure 32. A drop is seen initially due to MSR being more dominant over MgO carbonation before the temperature increases again as the latter reaction takes over.

For an inlet temperature of 350 °C, the temperature profile across the reactor length (using the same base case conditions, but adiabatic) is presented in Figure 33.

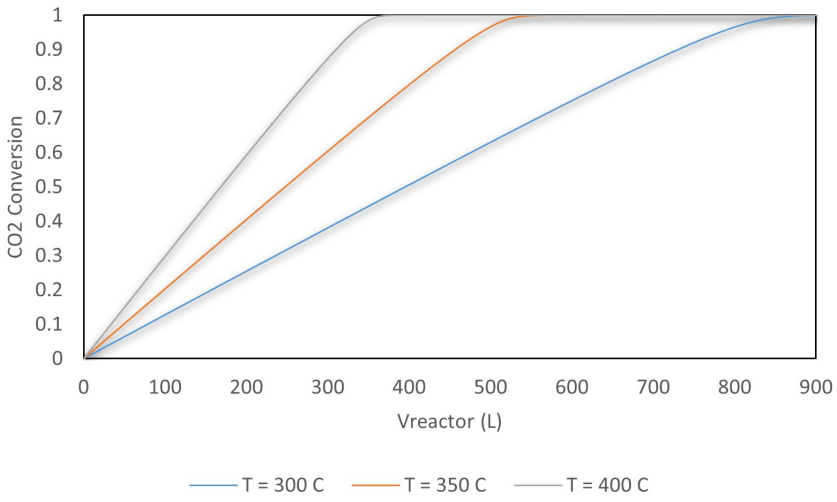

Figure 27: Effect of Temperature on CO_2 Conversion in MgO Carbonation for Inlet CO_2 = 357 kmol/hr at Total Pressure = 40 bar and ϵ = 5%.

3.3.2 Post-Reaction Composition

The effluent stream composition leaving the reactor operating at the base case conditions is seen in Table 6.

Table 6: Composition of the MSR + MgO Carbonation Reactor's Effluent at Base Case Conditions.

Component	**Mole Percent (%)**
H_2	79.8
H_2O	9
CO	8.6
CO_2	2.2
CH_3OH	0.35
N_2	0.006

Based on Table 6, the stream contains more than 8% CO for S/C = 1, which is far more than what is acceptable in a fuel cell (0.2 ppm). Although CO is the most critical, other components also exceed the limit set by the fuel cell. To control the CO levels in the outlet, S/C ratio can be increased. Figure 34 shows that with increasing the S/C, the CO fraction decreases significantly in the dry gas (after steam condensation). However, this decrease comes at the expense of the duty of H-1 (Check Figure 44). By increasing S/C from 1 to 2, the duty of the heater

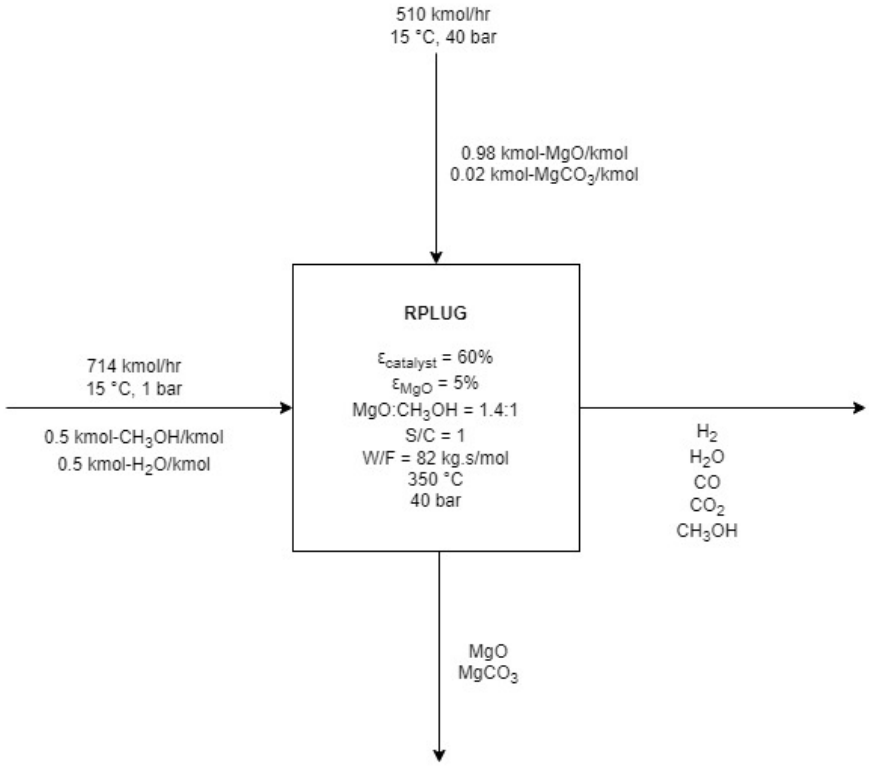

Figure 28: The Base Case Used for Comparison Reasons in a MSR Coupled With In-Situ CO_2 Conversion by MgO.

increases by 1.5 times.

As a result, it is crucial to choose the next process units in a way that produces a 99.97 mole% hydrogen purity with the individual components below the set limit by the fuel cell as seen in Table 1.

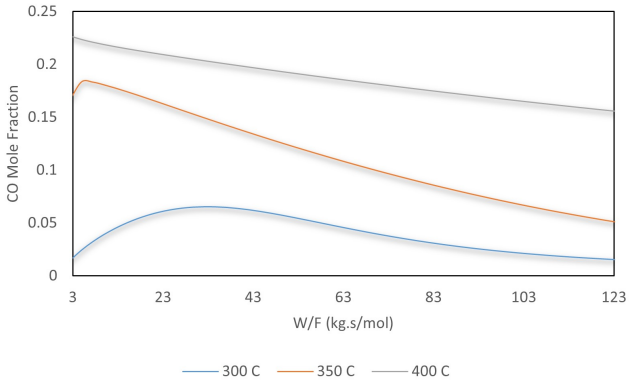

(a) CO Fraction

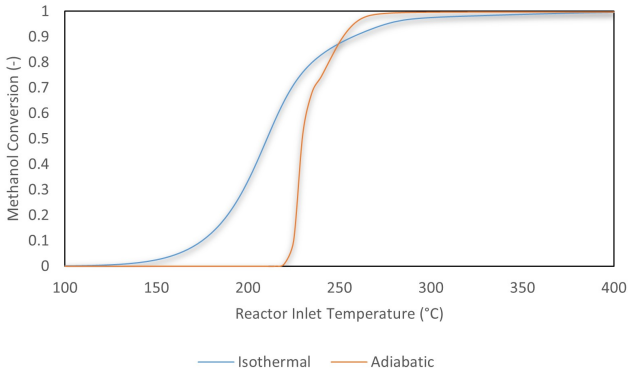

(b) Methanol Conversion

Figure 29: Temperature Effect on CO Fraction and MeOH Conversion in the Combined MSR + MgO Kinetic Reactor.

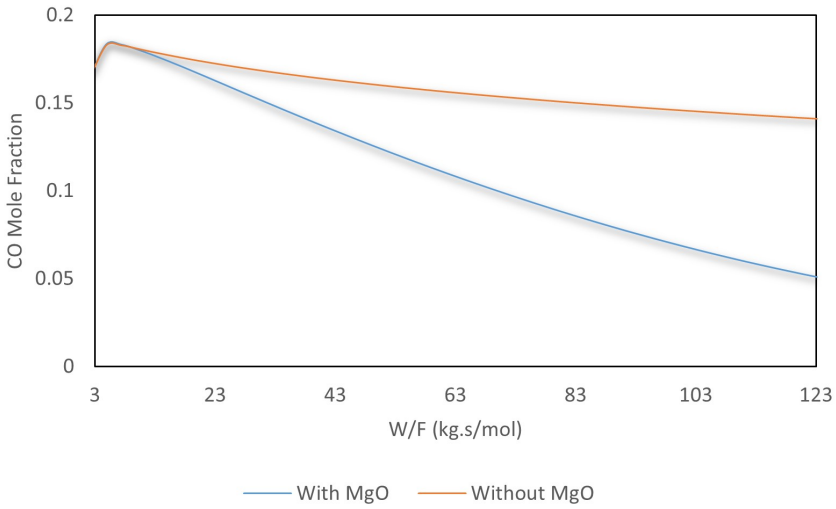

Figure 30: MgO Presence Effect on CO Fraction in the Combined MSR + MgO Kinetic Reactor.

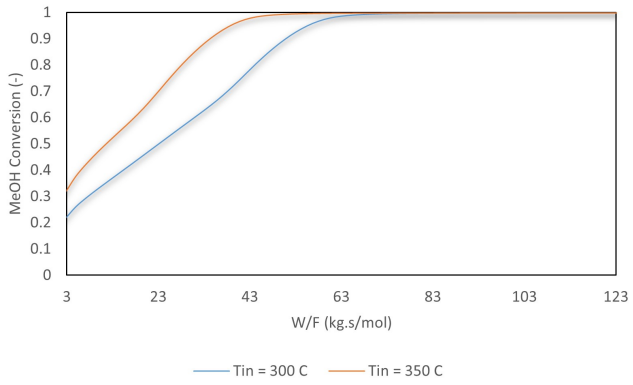

(a) Methanol Conversion

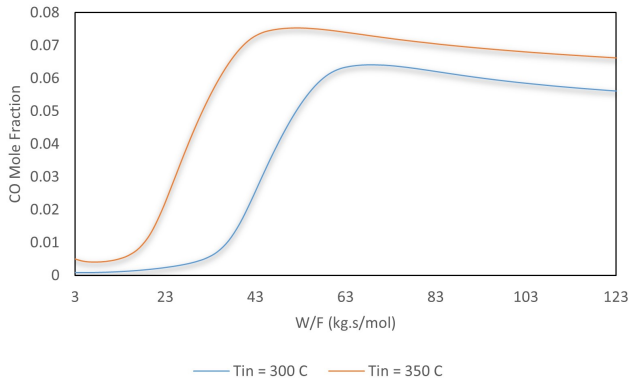

(b) CO Outlet Fraction

Figure 31: Adiabatic Reactor Effect on Methanol Conversion and CO Outlet Fraction in the Combined MSR + MgO Kinetic Reactor.

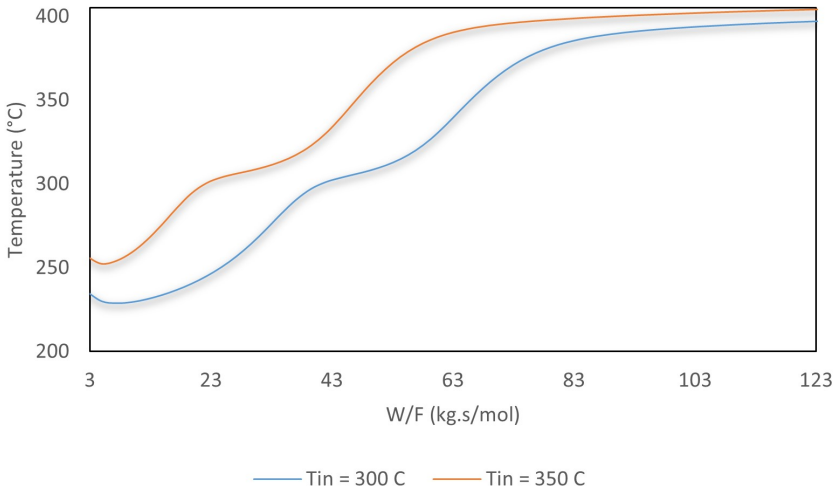

Figure 32: Effluent Temperature of the Adiabatic Reactor in the Combined MSR + MgO Kinetic Reactor.

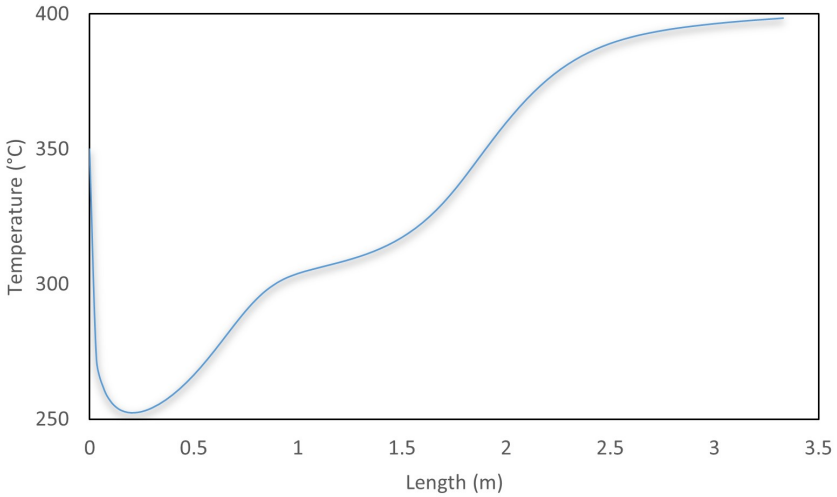

Figure 33: Temperature Profile Across the Length of the Adiabatic Operated Reactor in the Combined MSR + MgO Kinetic Reactor.

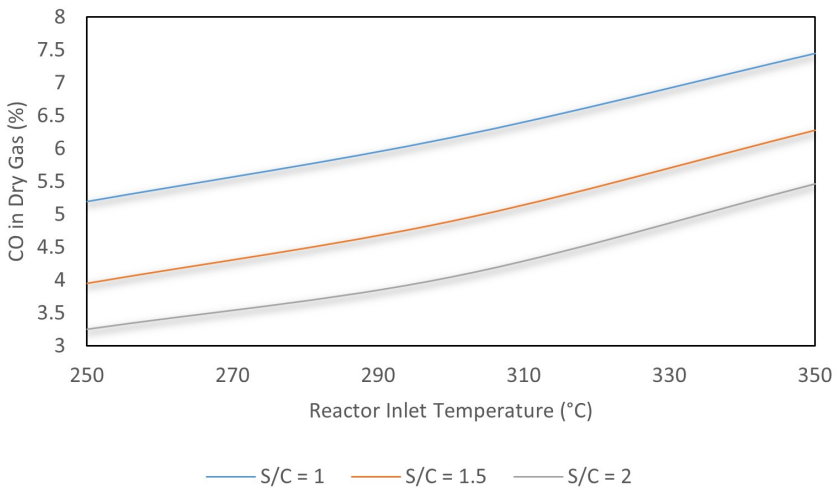

Figure 34: Temperature Profile Across the Length of the Adiabatic Operated Reactor in the Combined MSR + MgO Kinetic Reactor.

4. Process Design

In this section, the process design will take place by proposing the general block flow diagram (BFD) of the process based on the kinetic analysis. First, the BFD is made by considering that the hydrogen storage technology is methanol and the de-hydrogenation technique is the steam reforming of methanol coupled with in-situ CO_2 capture using MgO. After that, the process flow diagram (PFD) will be made by choosing the process behind each block in the BFD.

4.1 Block Flow Diagrams

The effluent leaving the MSR reactor is highly concentrated in hydrogen. However, the objective of the project is to use the hydrogen in a fuel cell according to ISO 14687-2. These standards are specified in Table 1 (only relevant components in this project).

As a result, it is wise to discuss first the composition of the stream leaving the MSR reactor. The final choices made by the thermodynamic analysis was to operate the MSR reactor at 350 °C, 40 bar, and S/C of 1. After that, the kinetic analysis concluded on the base case seen in Figure 28. The outlet composition of the reactor is presented in Table 6.

It is seen that the concentration of water, CO, and CO_2 should be reduced by around 100% to reach the requirement set by the fuel cell. For this reason, the Block Flow Diagram (BFD) was proposed as seen in Figure 35 for the sequence of the purification process after the MSR reaction.

After the MSR reactor, CO has to be removed or converted to CO_2. Methanol and steam are then condensed or phase separated. The CO_2 (including CO converted to CO_2) is removed to produce the required purity of hydrogen.

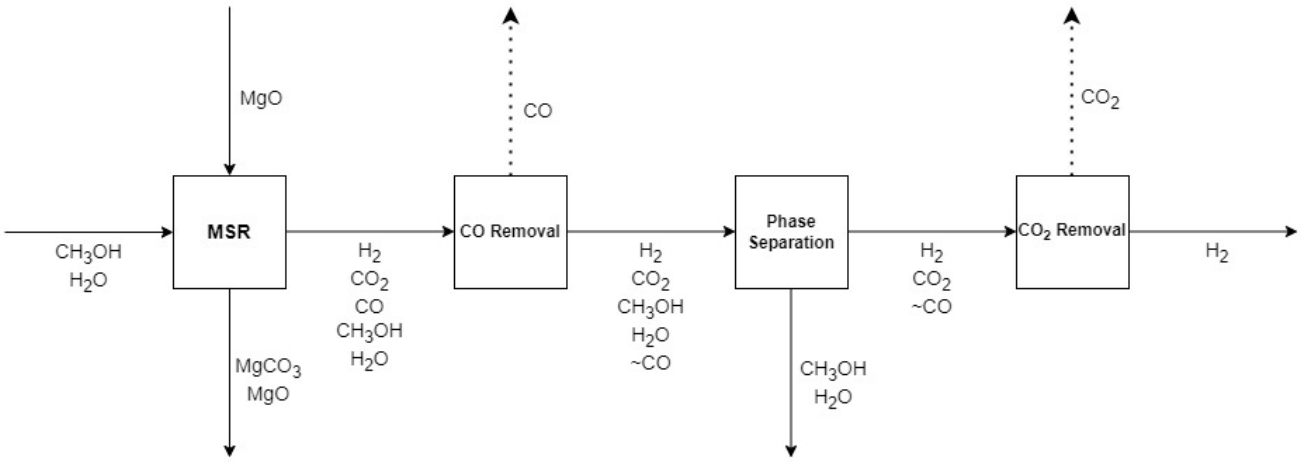

Figure 35: BFD Scenarios.

4.2 Post-MSR

After choosing the suitable sequence of units in the BFD, it is wise to look what the literature concludes on the specific units needed for each separation process. The first step will be to look for the available CO removal/conversion techniques. Only when this is clear, with their capacities, the unit for CO_2 removal will be easier to choose.

Figure 36 shows the available CO removal technologies available in the market or the industry. Membrane processes require expensive materials, high pressures, and not suitable for the very low CO quantity in the stream as no driving force exists between the sides of the membrane. CO oxidation have been studied in literature, and catalysts are showing effective results. However, the CO conversion by oxidation is not high unless a high temperature is used, which results in H_2 oxidation to water. WGS is used in a lot of industries, one of them is in ammonia production plants, to convert CO to CO_2. This process, although shows high conversions, can't achieve the desired CO removal alone. In addition, steam might need to be added to push the reaction towards CO_2, which end up diluting the hydrogen even further. As a result, WGS can be coupled with a pressure swing adsorption (PSA). The latter is a very promising and a well known process in the industry, especially for CO_2 removal from hydrogen streams in steam reforming off gas (SMROG) [5, 6, 37, 38].

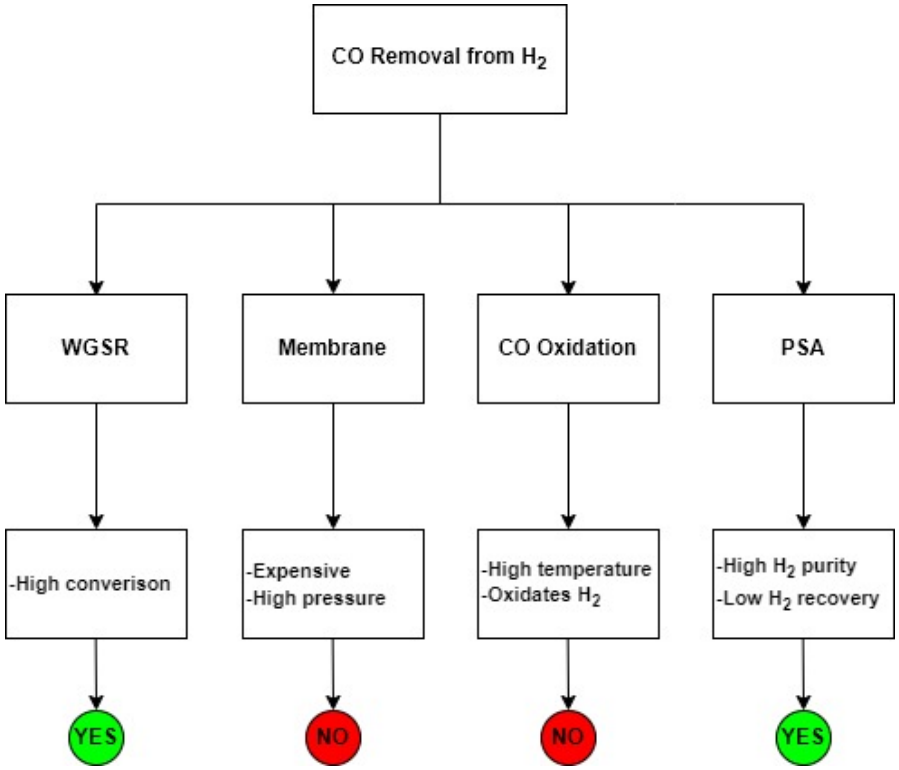

Figure 36: CO Removal/Conversion Technologies [5, 6].

For CO_2 removals, Zhemin Du et al. [37] compares different available PSA tech-

nologies for hydrogen purification for fuel cell applications. For a high hydrogen purity (≥99.99%) while maintaining a high hydrogen recovery rate (93 - 96%), Agueda et al. [7] proposes the UTSA-16, a metal-organic framework adsorbent. The feed contains 76% H_2, 17% CO_2, 4% CO, and rest CH_4. This feed is similar to the stream composition in Table 6, although not with H_2O and MeOH. The latter two components will be reduced to a negligible amount after the condensation. With this being said, it is important to note that the composition of CO and CO_2 is a big factor of a difference. For this reason, knowing the removal capacity of the adsorbent with respect to the individual components can help in estimating how a PSA can operate in this process. Due to data limitation, what is known from the publication [7] is that a 99.999% pure hydrogen stream is produced with the off-gas stream containing ∼60% CO_2 and 18% H_2 (which is approximate to 93% hydrogen recovery or 7% hydrogen loss). Fortunately, the off-gas containing 7 mole% of the inlet hydrogen can be burnt and used for providing energy for heating up the reactor inlet feed. On the other hand, what is crucial to notice from the concentration of the off-gas is the high affinity of the adsorbent towards CO_2. This means that converting CO to CO_2 is an important step before the PSA. Figure 37 gives a close illustration of the PSA used in the publication [7] where adsorption happens at 298 K and 16 bar.

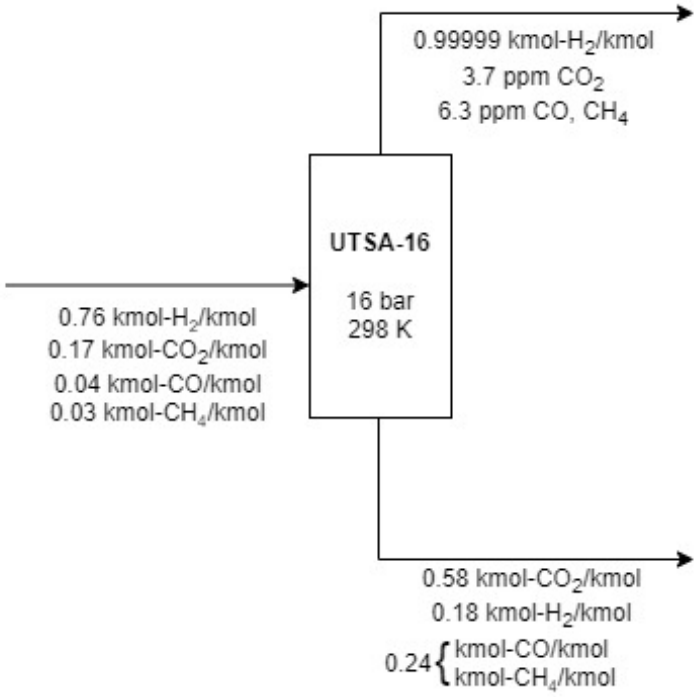

Figure 37: Estimation (Based on Available Data) of the Compositions of Inlet and Outlet of the PSA Studied by Agueda et al. [7].

From Figure 37, it can be seen that around 6 ppm of CO and CH_4, and 3 ppm of CO_2 are left in the hydrogen-rich stream. This is a huge reduction, yet is not acceptable by the fuel cell. However, it is important to note that the stream in the process (after the WGS to be added before the PSA) could contain much less CO and CO_2 than what the publication has. For now, it is concluded that this

adsorbent can remove more than 99.99% of CO_2, CO, MeOH, and water. Note that another adsorbent layer might be needed to remove water and methanol.

A set of BFD schematics were proposed as seen in Figure 38. It can be seen that Scenario A involves WGS to convert CO to CO_2 (as CO_2 specification is higher than that of CO for a fuel cell), and a PSA. Scenario B is needed if the outlet stream from the PSA still have some CO_2 left, which is not the case when using the UTSA-16 as an adsorbent in a PSA, as what could mostly be left is CO. Finally, Scenario C, where no WGS is needed, of which a PSA will not be enough to provide the required purity of hydrogen. As a result, from a general look, Scenario A seems the most suitable for now.

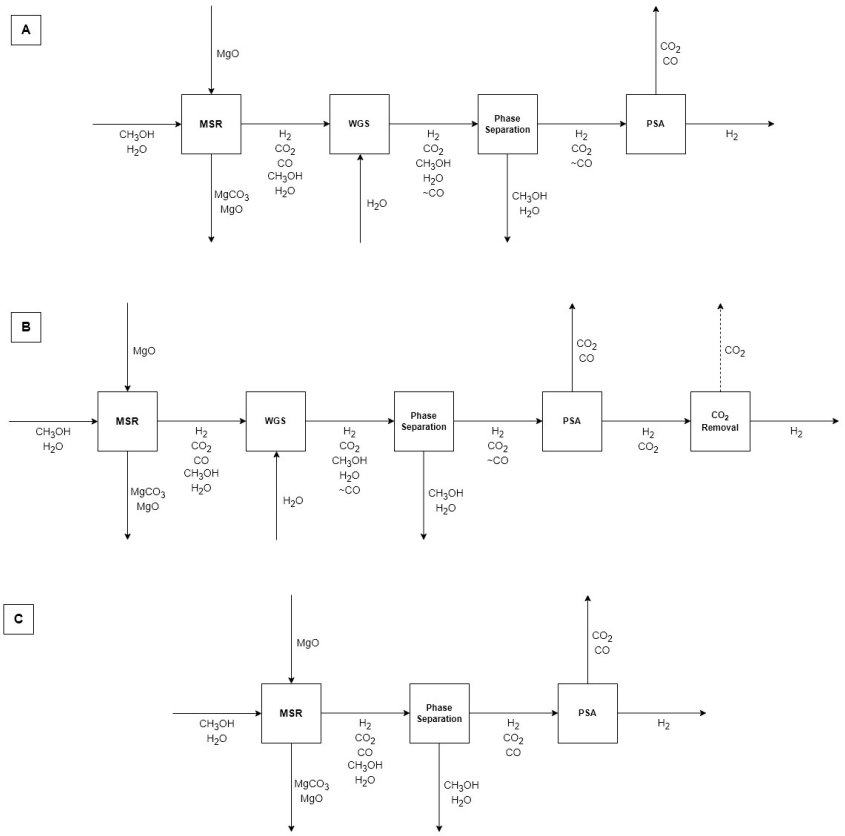

Figure 38: BFD Updated Sequence.

To conclude, a thermodynamic and kinetic analyses is suggested to be done on a WGS reactor post-MSR + MgO carbonation reactor. This will help in identifying to what extent can a WGS reduce the CO content before the PSA, helping the latter achieve the required purity needed for the fuel cell.

4.2.1 WGS Post-Reaction

As discussed earlier, the CO content in the outlet stream is 8%, which is far more than what can a fuel cell handle. The fuel cell specification of CO_2 is higher than that of CO. In addition, the PSA adsorbent's capacity towards CO_2 is much higher when compared to CO. As a result, a WGS is needed after the reactor to convert the CO to CO_2.

Thermodynamic and Kinetic Analyses of WGS

The effluent stream leaving the first reactor, which is MSR + MgO carbonation in-situ, goes into an RGIBBS to assess if the reaction can proceed on its own. Figure 39 shows the effect of temperature on the composition of the WGS reactor effluent. One could see that CO fraction can be reduced significantly when we operate at below 200 °C. In absolute values, the CO fraction goes from 8.6% to 0.05% at 200 °C. This is a huge reduction in CO content while CO_2 fraction increases by ∼1.4% absolute value.

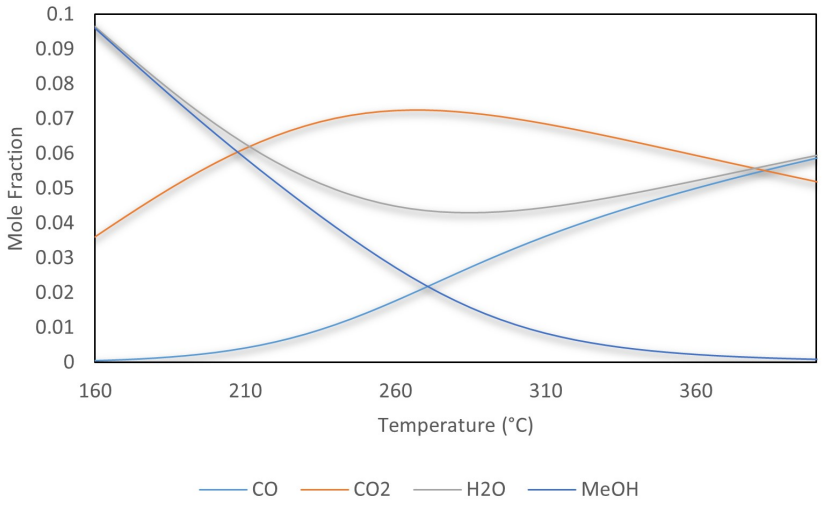

Figure 39: Thermodynamic Analysis of Temperature Effect on WGS Post-MSR + MgO Carbonation Kinetic Reactor of the Base Case.

To analyze the kinetic effect on the WGS, the same catalyst, $Cu/ZnO/Al_2O_3$ is used from Chapter 6. Equation 11 is used for the rate equation describing the WGS on the catalyst, while keeping the other rate equations for MSR and MD as this catalyst can catalyze these reactions as well. Looking at Figure 40, which shows the CO fraction of the effluent of the kinetic WGS reactor as a function of temperature and S/C at the inlet.

It can be seen in Figure 40 that around 175 °C - 250 °C, the CO fraction goes down to 0.15% - 1.4% at S/C equal to 1.5 and 1, respectively. In Table 7, the CO % after the WGS is compared to the CO % after the first MSR + MgO carbonation reactor.

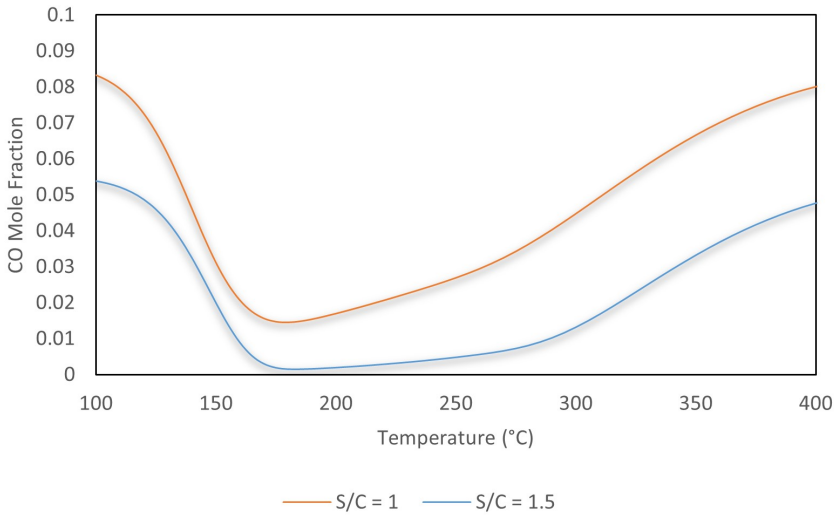

Figure 40: Kinetic Analysis of Temperature Effect on WGS Post-MSR + MgO Carbonation Kinetic Reactor of the Base Case.

Table 7: Effect of WGS on CO Content Post-MSR + MgO Kinetic Reactor.

S/C	**CO % After MSR + MgO Reactor**	**CO % After WGS Reactor**
1	8.6	1.4
1/5	5.5	0.15

The main conclusion drawn from here is that a WGS reactor could help reduce the CO content significantly before the PSA. As a continuation of the base case, the WGS kinetic reactor will operate at 180 °C according to the illustration in Figure 41. The double dash seen in the figure is to show that this is not the real position of the WGSR in the process. This is because the hot stream leaving the MSR reactor can be heat integrated to heat up the inlet feed of the reactor before entering the WGS at a lower temperature.

4.2.2 Possible Heat Integration

Operating the MSR reactor adiabatically helps in letting the MgO carbonation reaction cover up the energy required by the endothermic MSR. As it was presented earlier, the stream leaving the adiabatic reactor is at around 400 °C. After the MSR, it was decided to have a WGS reactor to reduce the CO content. The latter reactor operates at around 180 °C. To make use of the energy available in the hot stream leaving the first reactor, two scenarios can be followed as seen in Figures 42 and 43.

In the first scenario, the MSR effluent's energy is fully used in the heat exchanger

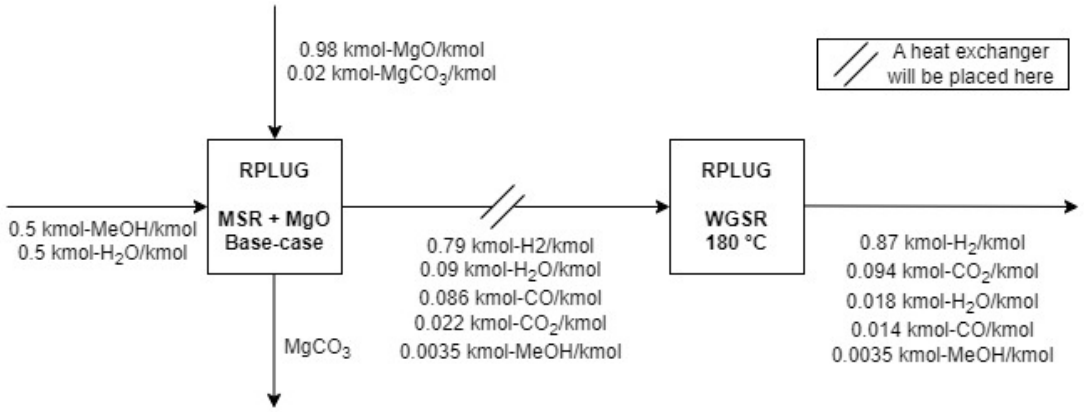

Figure 41: A Rough Illustration of the WGSR Post-MSR + MgO Carbonation Kinetic Reactor Position.

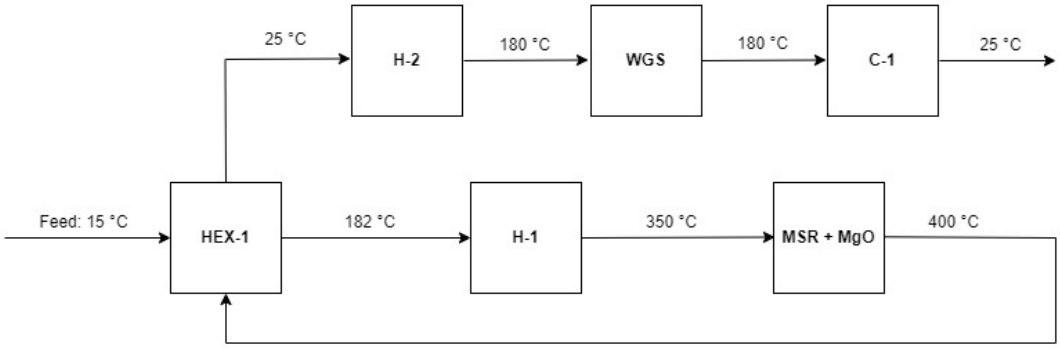

Figure 42: First Scenario for Heat Integrating MSR Effluent with Inlet.

with the feed. However, for the WGS, another heater is needed prior to the reactor. This is the same for the stream going into the MSR reactor as the temperature does not go above 220 °C after heat exchanging with the MSR effluent. Another cooler is needed to cool down the WGS effluent to the condenser temperature.

In the second scenario, the process looks more complex as two heat exchangers are used. The first one is used to keep the MSR effluent around 180 °C, so no extra heater is needed prior to the WGS reactor. However, the second heat exchanger will not be able to provide enough energy to heat up the feed to more than 130 °C due to temperature cross. With this, it can be seen that two heat exchangers, one heater, and a cooler (prior to the condenser and PSA) are needed. Table 8 shows a comparison between the two scenarios in terms of energy needed. Even with the integration, extra energy is needed. This is where the PSA plays a good role, as the off-gas which contains 7% of the PSA inlet stream's hydrogen, can be combusted to provide energy to the process.

To conclude this section, the second scenario will be used as it requires less energy overall and provides better heat integration of the MSR effluent stream. The cooler (C-1) temperature will be set to 25 °C as this is the PSA's operating temperature. At this temperature, 96% and 84% of the water and methanol, respectively, are

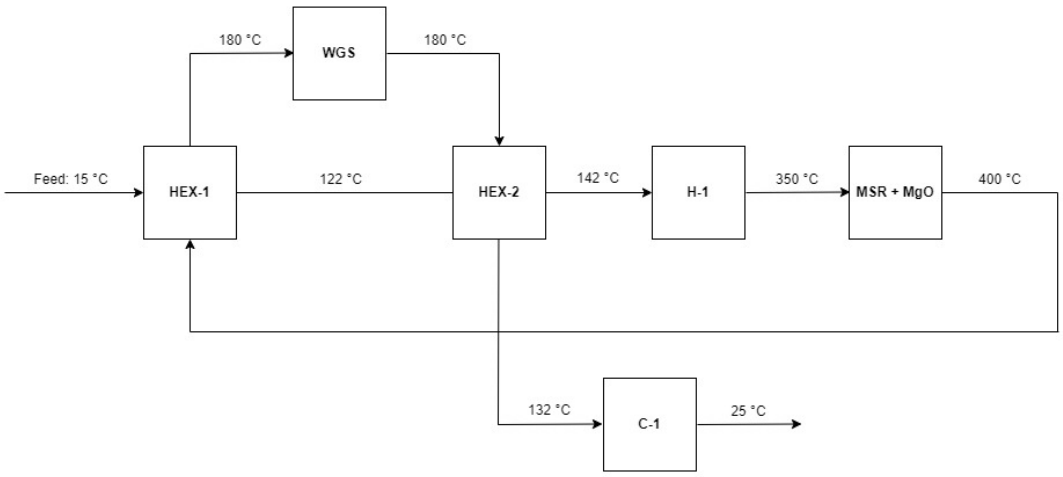

Figure 43: Second Scenario for Heat Integrating MSR Effluent with Inlet.

Table 8: Heat Integration Scenarios: Energy Requirement Comparison.

	Scenario 1 (kW)	**Scenario 2 (kW)**
H-1	8318.63	8619.52
H-2	1570.17	-
C-1	-1180.25	-1134.62

removed from the feed entering the condenser.

4.2.3 PSA and Combustion

In the PSA, an assumption that ≥99.99 removals is achieved for CO_2, CO, MeOH, and steam. This assumption is valid for CO_2 as it was a straight forward calculation made as reported in the publication. For MeOH and steam, the affinity of UTSA-16 towards these components is unknown, so this assumption can be valid only if a layer of alumina or silica gel is placed in the adsorption bed. For CO, and based on the publication by Agueda et al. [7], the affinity towards CO and methane is the almost the same. As a result, it was assumed that in the hydrogen saturated stream in Figure 36, 3.15 ppm of CO exist. This leaves us with a ≥99.99 removal of CO as well. Based on these assumptions, Table 9 shows the composition of the hydrogen saturated stream and that of the off-gas, before the combustor.

The table shows the required hydrogen purity is reached, while the individual components are present in the hydrogen-saturated stream below the limit set in Table 1. However, only CO still needs another final purification step, which could be done on a layer of zeolite, or activated carbon.

The off-gas can be used to provide energy for the extra heater needed before

Table 9: The Compositions of the Hydrogen-saturated and Off-gas Leaving the PSA.

Components	**Hydrogen-saturated (kmol/kmol)**	**Off-gas (kmol/kmol)**
H_2	0.99992	0.41
Impurities	**(ppm)**	**(mol%)**
H_2O	0.01	0.46
CO_2	1.39	49.13
CO	0.95	9.27
CH_3OH	0.02	0.11

the MSR reactor and to heat up the MgO feed. Combusting the off-gas at 25 °C and 1 bar results in 5750 kW of energy that can be used to cover 54% of the energy needed by the two heaters in the system (10.7 MW). Table 10 shows the inlet and outlet temperatures of the heaters and coolers in the system alongside their duties.

Table 10: Heaters and Coolers Inlet and Outlet Temperatures, and their Duties.

Unit	**Inlet Temperature** (°C)	**Outlet Temperature** (°C)	**Duty (MW)**
H-1	142	350	8.6
H-2	15	350	2.1
C-1	132	25	-1.1

To decide on an approximate sizing of the PSA, breakthrough curves are needed. However, one could estimate the diameter needed for the flowrate coming to the PSA. The volumetric flowrate is equal to 716.5 m^3/hr and the gas superficial velocity is set as 0.1 m/s. As a result, the diameter is calculated as 1.6 m. Assuming a length to diameter ratio of 5, the length of the adsorption bed can go up to 8 m as seen in Table 11.

The saturation time alongisde the length needed to exceed the maximum pressure drop is discussed in details in Chapter in the Appendix. As this is an approximation, it is recommended to do a detailed design on a dynamic software such as Aspen Adsorption to obtain better results as mass transfer limitations, adsorption isotherms, alongside the multi-component competition is taken into account.

Table 11: Diameter and Length for PSA.

Parameter	**Value**
Volumetric Flow (m^3/hr)	716.5
u (m/s)	0.1
A (m^2)	2
D (m)	1.6
L (m)	8
$\rho_{adsorbent}$ (kg/m^3)	1171

4.3 Process Flow Diagram: Flowsheet Analysis

The composition of the MSR and WGS reactors' effluents are known as well as the PSA removal capacity. In addition, the heat integration between MSR's effluent and feed is set and known. As a result, the final process flow diagram (PFD) is presented in Figure 44.

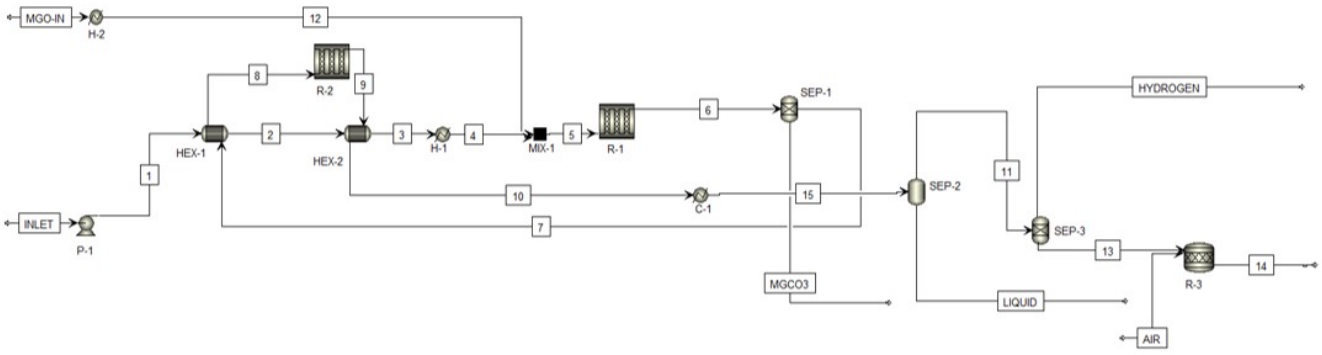

Figure 44: The Final Process Flow Diagram (PFD).

Methanol and steam are fed at 1 bar and 15 °C. First, the feed is pumped to 40 bar in P-1 and then is heat exchanged with the MSR effluent stream to a temperature of 122 °C in HEX-1. An extra heater (H-1) is needed to increase the temperature up to 350 °C (refer to the base case in Figure 28). On the other side, the MgO solid is fed at 15 °C and 40 bar. Then, the hot and pressurized gas stream is mixed with the solid MgO stream and fed to the first reactor, MSR + MgO carbonation kinetic reactor (R-1).

After the reaction takes place, the effluent is phase separated to remove all solids, MgO and $MgCO_3$, in SEP-1. The gas phase heat exchanges with the feed in HEX-1 as mentioned earlier, until reaching a temperature of 180 °C, at which the WGS

reactor (R-2) operates. Then, the gas stream cools down to 25 °C in C-1 as at this temperature, water and methanol condensation take place in SEP-2. Consequently, the gas stream goes into a PSA (SEP-3), where hydrogen is purified. The off-gas (stream 13) goes into R-3 to react with air and provide energy for the process.

5. Conclusion

Hydrogen emerges as a highly promising option for replacing conventional fossil fuels in energy applications due to its unparalleled energy-to-mass ratio and clean combustion. Renewable production methods like wind and solar power enhance its appeal as an eco-friendly alternative. However, the challenge of efficient hydrogen storage persists due to its low volumetric energy density. Solutions involving pressure and liquefaction offer increased density but face hurdles like energy-intensive processes and material requirements.

Methanol stands out among hydrogen storage choices with its notable theoretical hydrogen capacity of up to 18.75 wt.%. Its affordability, wide availability, and ease of handling due to a moderate boiling point contribute to its appeal. Its industrial reversibility for hydrogen release further adds to its attractiveness. Nonetheless, methanol's handling toxicity and potential CO/CO_2 generation during processes like thermal decomposition pose concerns. Yet, its potential as a robust hydrogen storage solution remains evident.

To overcome methanol's drawback of CO/CO_2 generation, MgO is proposed to capture CO_2 and form $MgCO_3$. Therefore, the process that was studied is methanol steam reforming coupled with MgO carbonation for CO_2 capture. The main answers to the research questions of this work are:

- MgO's presence in-situ is capable of capturing CO_2 as it is produced, but it is kinetically limited and slow. Therefore, promoted MgO was used. The latter converted 93% of the produced CO_2 from MSR to $MgCO_3$.
- MSR achieved 99.7% conversion of methanol at S/C = 1 in presence of MgO when the reactor was adiabatic at base case conditions (T_{in} = 350 °C).
- At base case conditions, the MSR reactor's effluent contained 79.8% hydrogen. The most concerning part was that this stream contained 8% CO that needs to be removed down to 0.2 ppm.
- Post-reaction, a WGS and a PSA are needed to achieve the desired purity of hydrogen. The WGS reactor reduced the CO content from 8% down to 1.4%. The PSA was able to reduce the CO content significantly. However, another cleaning unit is needed for more CO removals after the PSA.
- In an adiabatic operated MSR + MgO kinetic reactor, the MgO carbonation reaction increased the reactor temperature from 350 °C to 400 °C. This showed that the MgO was able to cover up for the MSR energy duty.
- The MSR reactor's effluent was not able to provide enough energy for the feed. This stream covered 54% of the energy needed by the extra heaters for MSR feed and heating up the MgO feed, while 4.9 MW of excess energy is still needed.

6. Recommendations

More work could be done to enhance the accuracy of the Aspen Model used in this work. These include:

- Design the reactor in details by choosing the best configuration. The reactor operation is complex with MSR when combined with MgO, as a catalyst exist in the bed as well.
- The PSA had some assumptions including the % removals of the impurities and the affinity towards methanol and water. A recommendation would be to simulate the PSA in details using either MATLAB or Aspen Adsorption to obtain accurate results of the removal capacity, bed sizing, and cycle duration.
- The pressure effect on the MgO carbonation rate was assumed to be linear. However, experimental work on this relation would help in shaping a better understanding of the rate equation at high pressures. In addition to that, effect of steam on MgO was not considered. As literature states that it could improve the kinetics of carbonation, it is also suggested to consider this in future work.
- Steam can have negative effects on the $Cu/ZnO/Al_2O_3$ catalyst, which were not taken into account in this project.
- The reverse process of decomposing $MgCO_3$ to produce CO_2 and MgO again can be studied. In this way, methanol is produced again and a cycle is made.

References

[1] G. Garcia, E. Arriola, W.-H. Chen, and M. D. De Luna, "A comprehensive review of hydrogen production from methanol thermochemical conversion for sustainability," *Energy*, vol. 217, p. 119384, 2021.

[2] H. Ebrahimi and M. Rahmani, "A new design for co2 capture and usage in a syngas production unit by carbonate chemical looping," *Journal of Natural Gas Science and Engineering*, vol. 36, pp. 241–251, 2016.

[3] R. Chang, X. Wu, O. Cheung, and W. Liu, "Synthetic solid oxide sorbents for co 2 capture: state-of-the art and future perspectives," *Journal of Materials Chemistry A*, vol. 10, no. 4, pp. 1682–1705, 2022.

[4] H. Cui, Q. Zhang, Y. Hu, C. Peng, X. Fang, Z. Cheng, V. V. Galvita, and Z. Zhou, "Ultrafast and stable co2 capture using alkali metal salt-promoted mgo–caco3 sorbents," *ACS applied materials & interfaces*, vol. 10, no. 24, pp. 20611–20620, 2018.

[5] S. Takenaka, T. Shimizu, and K. Otsuka, "Complete removal of carbon monoxide in hydrogen-rich gas stream through methanation over supported metal catalysts," *International Journal of Hydrogen Energy*, vol. 29, no. 10, pp. 1065–1073, 2004.

[6] S. Srinivas, A. Dhingra, H. Im, and E. Gulari, "A scalable silicon microreactor for preferential co oxidation: performance comparison with a tubular packed-bed microreactor," *Applied Catalysis A: General*, vol. 274, no. 1-2, pp. 285–293, 2004.

[7] V. I. Agueda, J. A. Delgado, M. A. Uguina, P. Brea, A. I. Spjelkavik, R. Blom, and C. Grande, "Adsorption and diffusion of h2, n2, co, ch4 and co2 in utsa-16 metal-organic framework extrudates," *Chemical Engineering Science*, vol. 124, pp. 159–169, 2015.

[8] M. Aziz, A. T. Wijayanta, and A. B. D. Nandiyanto, "Ammonia as effective hydrogen storage: A review on production, storage and utilization," *Energies*, vol. 13, no. 12, p. 3062, 2020.

[9] M. Niermann, A. Beckendorff, M. Kaltschmitt, and K. Bonhoff, "Liquid organic hydrogen carrier (lohc)–assessment based on chemical and economic properties," *International Journal of Hydrogen Energy*, vol. 44, no. 13, pp. 6631–6654, 2019.

[10] B. Ekwurzel, J. Boneham, M. W. Dalton, R. Heede, R. J. Mera, M. R. Allen, and P. C. Frumhoff, "The rise in global atmospheric co2, surface temperature, and sea level from emissions traced to major carbon producers," *Climatic Change*, vol. 144, no. 4, pp. 579–590, 2017.

[11] U. N. F. C. on Climate Change. Secretariat, *United Nations framework convention on climate change*. UNFCCC, 1992.

[12] S. Z. Al Ghafri, S. Munro, U. Cardella, T. Funke, W. Notardonato, J. M. Trusler, J. Leachman, R. Span, S. Kamiya, G. Pearce, *et al.*, "Hydrogen liquefaction: a review of the fundamental physics, engineering practice and future opportunities," *Energy & environmental science*, vol. 15, no. 7, pp. 2690–2731, 2022.

[13] T. H. Ulucan, S. A. Akhade, A. Ambalakatte, T. Autrey, A. Cairns, P. Chen, Y. W. Cho, F. Gallucci, W. Gao, J. B. Grinderslev, *et al.*, "Hydrogen storage in liquid hydrogen carriers: recent activities and new trends," *Progress in Energy*, vol. 5, no. 1, p. 012004, 2023.

[14] M. Yang, R. Hunger, S. Berrettoni, B. Sprecher, and B. Wang, "A review of hydrogen storage and transport technologies," *Clean Energy*, vol. 7, no. 1, pp. 190–216, 2023.

[15] A. Eftekhari and B. Fang, "Electrochemical hydrogen storage: opportunities for fuel storage, batteries, fuel cells, and supercapacitors," *International Journal of Hydrogen Energy*, vol. 42, no. 40, pp. 25143–25165, 2017.

[16] R. Chamoun, U. B. Demirci, and P. Miele, "Cyclic dehydrogenation–(re) hydrogenation with hydrogen-storage materials: An overview," *Energy Technology*, vol. 3, no. 2, pp. 100–117, 2015.

[17] Q. Lai, M. Paskevicius, D. A. Sheppard, C. E. Buckley, A. W. Thornton, M. R. Hill, Q. Gu, J. Mao, Z. Huang, H. K. Liu, *et al.*, "Hydrogen storage materials for mobile and stationary applications: current state of the art," *ChemSusChem*, vol. 8, no. 17, pp. 2789–2825, 2015.

[18] M. Bui, C. S. Adjiman, A. Bardow, E. J. Anthony, A. Boston, S. Brown, P. S. Fennell, S. Fuss, A. Galindo, L. A. Hackett, *et al.*, "Carbon capture and storage (ccs): the way forward," *Energy & Environmental Science*, vol. 11, no. 5, pp. 1062–1176, 2018.

[19] I. I. Cheema and U. Krewer, "Operating envelope of haber–bosch process design for power-to-ammonia," *RSC advances*, vol. 8, no. 61, pp. 34926–34936, 2018.

[20] P. Peng, J. Su, and H. Breunig, "Benchmarking plasma and electrolysis decomposition technologies for ammonia to power generation," *Energy Conversion and Management*, vol. 288, p. 117166, 2023.

[21] A. M. Ranjekar and G. D. Yadav, "Steam reforming of methanol for hydrogen production: A critical analysis of catalysis, processes, and scope," *Industrial & Engineering Chemistry Research*, vol. 60, no. 1, pp. 89–113, 2021.

[22] D. Berstad, R. Anantharaman, R. Blom, K. Jordal, and B. Arstad, "Ngcc post-combustion co2 capture with ca/carbonate looping: Efficiency dependency on sorbent properties, capture unit performance and process configuration," *International Journal of Greenhouse Gas Control*, vol. 24, pp. 43–53, 2014.

[23] J. Blamey, E. Anthony, J. Wang, and P. Fennell, "The use of the calcium looping cycle for post-combustion co2 capture," *Prog. Energy Combust. Sci*, vol. 36, pp. 260–279, 2010.

[24] M. E. Boot-Handford, J. C. Abanades, E. J. Anthony, M. J. Blunt, S. Brandani, N. Mac Dowell, J. R. Fernández, M.-C. Ferrari, R. Gross, J. P. Hallett, *et al.*, "Carbon capture and storage update," *Energy & Environmental Science*, vol. 7, no. 1, pp. 130–189, 2014.

[25] A. A. Olajire, "A review of mineral carbonation technology in sequestration of co2," *Journal of Petroleum Science and Engineering*, vol. 109, pp. 364–392, 2013.

[26] W. Gao, L. Sun, and Q. Wang, "Mgo-based intermediate-temperature co2 adsorbents," in *Pre-combustion Carbon Dioxide Capture Materials*, pp. 61–143, 2018.

[27] F. Donat and C. R. Müller, "Prospects of mgo-based sorbents for co2 capture applications at high temperatures," *Current Opinion in Green and Sustainable Chemistry*, p. 100645, 2022.

[28] G. Ji, H. Yang, M. Z. Memon, Y. Gao, B. Qu, W. Fu, G. Olguin, M. Zhao, and A. Li, "Recent advances on kinetics of carbon dioxide capture using solid sorbents at elevated temperatures," *Applied energy*, vol. 267, p. 114874, 2020.

[29] A.-T. Vu, K. Ho, S. Jin, and C.-H. Lee, "Double sodium salt-promoted mesoporous mgo sorbent with high co2 sorption capacity at intermediate temperatures under dry and wet conditions," *Chemical Engineering Journal*, vol. 291, pp. 161–173, 2016.

[30] Y. Qiao, J. Wang, Y. Zhang, W. Gao, T. Harada, L. Huang, T. A. Hatton, and Q. Wang, "Alkali nitrates molten salt modified commercial mgo for intermediate-temperature co2 capture: optimization of the li/na/k ratio," *Industrial & Engineering Chemistry Research*, vol. 56, no. 6, pp. 1509–1517, 2017.

[31] J. Fagerlund, J. Highfield, and R. Zevenhoven, "Kinetics studies on wet and dry gas–solid carbonation of mgo and mg (oh) 2 for co 2 sequestration," *RSC advances*, vol. 2, no. 27, pp. 10380–10393, 2012.

[32] R. V. Siriwardane and R. W. Stevens Jr, "Novel regenerable magnesium hydroxide sorbents for co2 capture at warm gas temperatures," *Industrial & Engineering Chemistry Research*, vol. 48, no. 4, pp. 2135–2141, 2009.

[33] D. P. Butt, K. S. Lackner, C. H. Wendt, S. D. Conzone, H. Kung, Y.-C. Lu, and J. K. Bremser, "Kinetics of thermal dehydroxylation and carbonation of magnesium hydroxide," *Journal of the American Ceramic Society*, vol. 79, no. 7, pp. 1892–1898, 1996.

[34] Y. Lwin, W. R. W. Daud, A. B. Mohamad, and Z. Yaakob, "Hydrogen production from steam–methanol reforming: thermodynamic analysis," *International journal of hydrogen energy*, vol. 25, no. 1, pp. 47–53, 2000.

[35] I. Staffell, P. Dodds, D. Scamman, A. V. Abad, N. Dowell, K. Ward, P. Agnolucci, L. Papageorgiou, N. Shah, and P. Ekins, *The role of hydrogen and fuel cells in future energy systems.* Hydrogen and Fuel Cell Research Hub, 2017.

[36] B. A. Peppley, J. C. Amphlett, L. M. Kearns, and R. F. Mann, "Methanol–steam reforming on cu/zno/al2o3 catalysts. part 2. a comprehensive kinetic model," *Applied Catalysis A: General*, vol. 179, no. 1-2, pp. 31–49, 1999.

[37] Z. Du, C. Liu, J. Zhai, X. Guo, Y. Xiong, W. Su, and G. He, "A review of hydrogen purification technologies for fuel cell vehicles," *Catalysts*, vol. 11, no. 3, p. 393, 2021.

[38] G. Moral, R. Ortiz-Imedio, A. Ortiz, D. Gorri, and I. Ortiz, "Hydrogen recovery from coke oven gas. comparative analysis of technical alternatives," *Industrial & Engineering Chemistry Research*, vol. 61, no. 18, pp. 6106–6124, 2022.

[39] S. Sa, J. M. Sousa, and A. Mendes, "Steam reforming of methanol over a cuo/zno/al2o3 catalyst, part i: Kinetic modelling," *Chemical Engineering Science*, vol. 66, no. 20, pp. 4913–4921, 2011.

[40] W. L. McCabe, J. C. Smith, and P. Harriott, *Unit operations of chemical engineering*, vol. 5. McGraw-hill New York, 1993.

Appendix

Hydrogen Storage Systems: Comparison Criteria

The criteria followed for comparing hydrogen storage systems discussed in this project is seen in Table 12.

Table 12: Criteria Explanation for Hydrogen Storage Systems [9].

Frame conditions	**Criteria**
Storage	Storage capacity (wt.%) and volumetric energy density (kWh/L)
Availability	Cheap and available
Toxicity	Estimated by Toxicity Potential Indicator (TPI) from 0 (not toxic) to 100 (toxic)
De-hydrogenation temperature	The lower the temperature, the easier it is to cover the demand
Energy demand	Mainly determined by the de-hydrogenation heat demand and the heat integration possibility between loading and unloading
Material handling	Ideal case of low melting and high boiling point, keeping it liquid throughout the whole process
Process design	High melting points, low boiling points, low ignition temperatures, and low flashpoints carriers are undesirable due to the need for extra separation units and safety requirements
Stability	The carrier should be stable across cycles by showing high turnover number, long operation time, and fast reaction rates
Technical readiness	The Technology Readiness Level (TRL) shows how developed the operating system is on a rating from 1 (less developed) to 9 (most developed)

Physical Properties

The components seen in this project have properties listed in Table 13. These properties were obtained from different sources including Aspen Plus and NIST Database.

From Cui et al. [4], the composition of the AMS-$Mg_{95}Ca_5$ is given as in Table 14.

Table 13: Physical Properties of Different Components

Property	**H_2**	**CO**	**CO_2**	**CH_4**	**CH_3OH**	**H_2O**
Melting point (K)	14.00	68.15	216.50	90.70	175.50	273.15
Boiling point (K)	20.37	81.64	194.66	111.65	337.85	373.15
Molecular weight (g/mol)	2.01	28.01	44.01	16.04	32.04	18.01
Density (kg/m^3)	0.08	1.13	1.78	0.65	786.47 (l)	997.01 (l)
Viscosity (μPa·s)	8.89	17.76	14.9	11.07	544.89 (l)	893.07 (l)
Solubility in water (mg/kg-H_2O)	1.55	25.00	1500.00	Insoluble	Miscible	Miscible

MgO Carbonation Kinetic Model and Validation

This section discusses in details how the kinetic rate equation for MgO carbonation was obtained from the paper presented by Cui et al. [4].

The kinetic equation follows Equation 12 where rCO_2 is the reaction rate of Equation 6 in $kmol/(m^3 \cdot s)$, k is the kinetic constant in $seconds^{-1}$, ΔPCO_2 is the driving force for the reaction, and S is the conversion factor to correct the rate units (See Equation 13). Note that the data obtained from the paper is at 1 bar, so an assumption is made to present the pressure effect on the rate since it is unknown. A linear relation between ΔPCO_2 and rCO_2 is made where P_{ref} is equal to 1 bar.

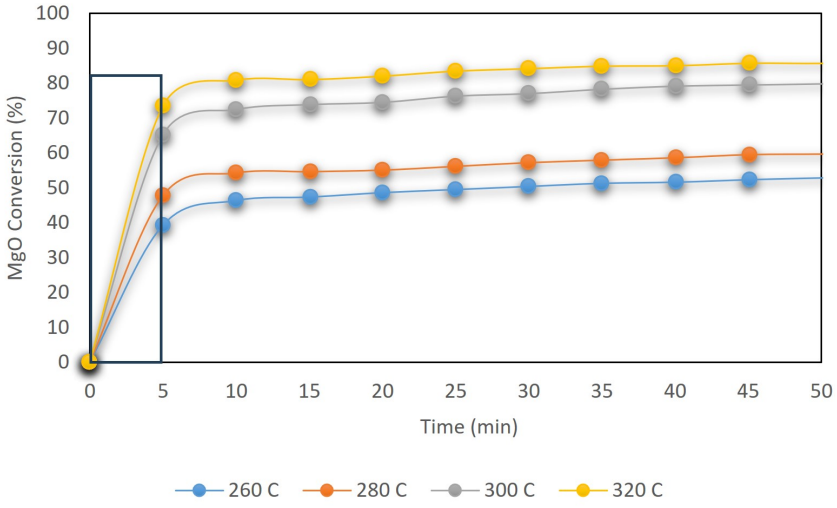

Figure 45: Experimental MgO Conversion Versus Time for Equation 6 Using AMS-$Mg_{95}Ca_5$ at 1 bar Total Pressure [4].

Table 14: AMS-$Mg_{95}Ca_5$ Skeletal and Bulk Density Calculations from Composition and Data by Cui et al. [4].

Component	**Mass Percent (%)**	**Skeletal Density (kg/m^3)**
MgO	65.7	3580
$CaCO_3$	8.7	2710
$LiNO_3$	5.2	2380
KNO_3	9.8	2110
Na_2CO_3	4.6	2540
K_2CO_3	6	2430
Skeletal Density (kg/m^3)		**3181**
Bulk Density (kg/m^3)		**1907 (at 40% porosity)**

$$rCO_2 = S \cdot k \cdot \frac{\Delta P_{CO2}}{P_{ref}} \tag{12}$$

$$S = x_{MgO} \cdot \rho_{MgO} \cdot \epsilon \cdot MW_{MgO} \tag{13}$$

After fitting the straight lines from Figure 45, the kinetic constants are obtained at each temperature as seen in Table 15 and Figure 46.

Table 15: MgO Carbonation Reaction Kinetic Constant After 5 Minutes.

Temperature (K)	**k (min^{-1})**
533	7.8
553	9.5
573	13
593	14.7

The kinetic constant is a function of temperature according to Arrhenius Equation in Equation 14. To obtain k_0 and E_a, Equation 15 is used in Figure 46.

$$k = k_0 \cdot e^{\frac{-Ea}{(R \cdot T)}} \tag{14}$$

$$Lnk = -\frac{Ea}{R} \cdot \frac{1}{T} + Ln(k_0) \tag{15}$$

Where k is the kinetic constant in min^{-1}, k_0 is the pre-exponential factor in min^{-1}, Ea is the activation energy in $kJ \cdot mol^{-1}$, T is the temperature in Kelvin, and R is the ideal gas constant in $J \cdot mol^{-1} \cdot K^{-1}$.

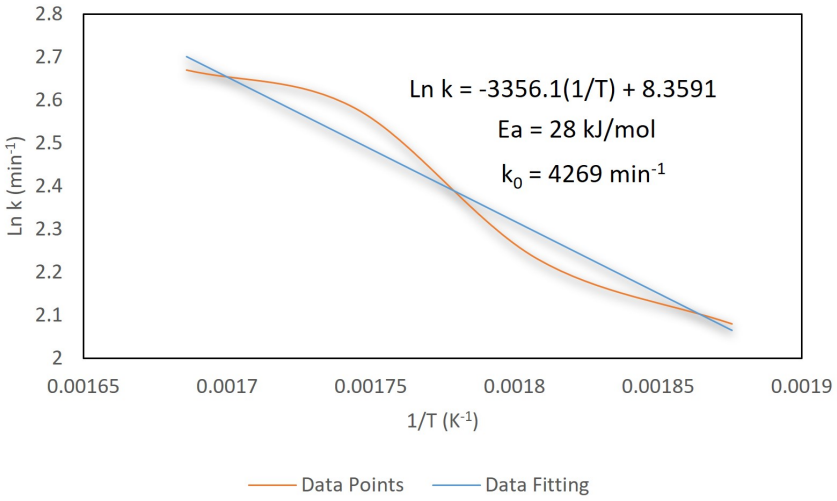

Figure 46: Ln k Versus 1/T for MgO Carbonation after 5 Minutes.

The experiment done by Cui et al. [4] for MgO carbonation is in a TGA while on Aspen Plus, a Plug Flow Reactor (R-PLUG) is used. To control kinetics in a way that mimics the experimental observations, MgO is used in excess. Looking at Figure 45, it can be seen that the highest MgO conversion does not exceed 75% at 320 °C and 1 bar total pressure. Higher CO_2 pressures will lead to a faster rate and higher conversions. As a result, operating at $P > 20$ bar will definitely lead to better performance in terms of CO_2 capture. However, because the data of pressure effect on MgO carbonation is lacking, it is assumed the best case performance is an MgO conversion of 72% as long as the partial pressure of CO_2 does not drop below 1 bar. Therefore, 40% excess MgO is used to ensure full conversions of CO_2 is possible.

MSR Kinetic Model and Validation

To validate the model used in Aspen Plus for MSR, experimental work on MSR presented by Sa´ et al. [39] and Peppley et al. [36] are used. These experiments show the effect of temperature and pressure on methanol conversion for a feed of methanol and steam. First, the catalyst amount in kg to inlet methanol flowrate (W/F), or contact time, is validated with experimental data as in Figure 47. To vary W/F, the flowrate is fixed and mass of catalyst used was changed. Although a small deviation is seen, the model seems to predict the behavior at 1 bar well.

Second, the pressure effect should be validated as in an MSR, a high pressure process is required to achieve higher hydrogen partial pressures. Figure 48 shows the effect of pressure on methanol conversion for experimental work presented by

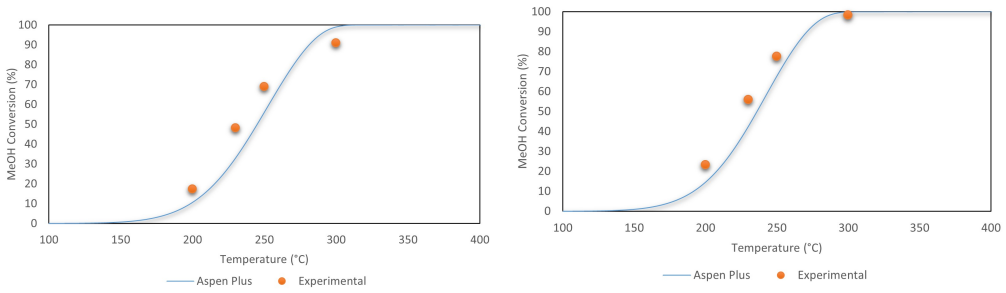

(a) W/F = 10 kg·s·mol^{-1} (b) W/F = 15 kg·s·mol^{-1}

Figure 47: MSR Kinetic Model Validation Using Methanol Conversion Versus Temperature for $m_{catalyst}$ = 1 kg and S/C = 1.5.

Peppley et al. [36] versus Aspen Plus.

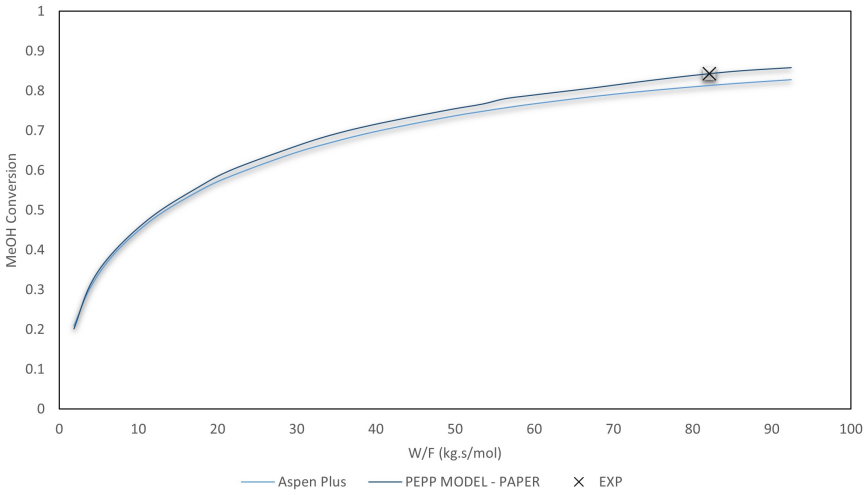

Figure 48: MSR Kinetic Model Validation for Pressure Effect Using Methanol Conversion Versus W/F at 39 bar and 533 K for $m_{catalyst}$ = 1 kg and S/C = 1.

To test the equilibrium extents of the model, results from Rgibbs are used next to the kinetic reactor. Figure 49 compares the equilibrium results from Rgibbs with varying the catalyst amount to increase the W/F in the kinetic model. By increasing the mass of catalyst from 1 kg to 1000 kg, the maximum conversion seen by the model overlaps with the equilibrium curve from Rgibbs. This clearly shows that the model does not exceed the equilibrium extent of the reaction.

Overall, the model results from Aspen Plus agrees largely with the experimental observations. As a result, this model is validated and will be used in the simulations.

The kinetic rate used in Aspen Plus has the unit kmol/m^3·s, so the RPLUG requires input of volume instead of mass of catalyst. To change the volume of the reactor in correspondence with a fixed W/F value, Equations 16 and 17 are

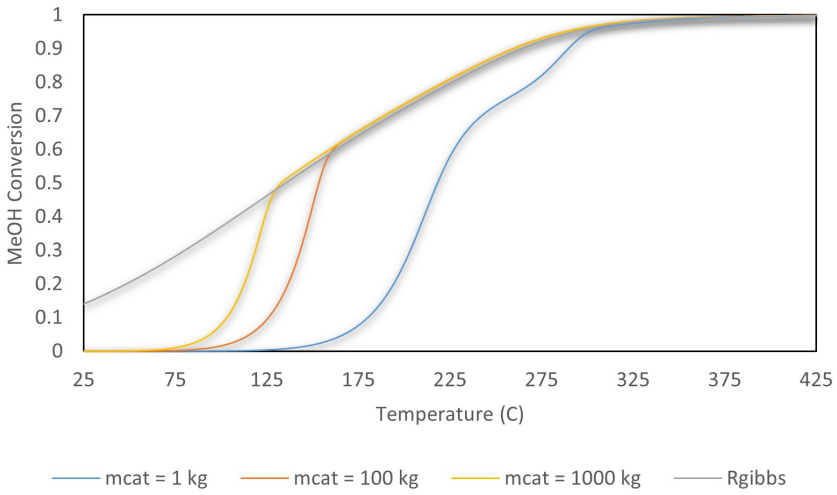

Figure 49: MSR Kinetic Model Validation for Equilibrium Extents at 39 bar for $m_{catalyst}$ = 1 kg - 1000 kg and S/C = 1.

used. Note that ρ_{MgO} is obtained based on reported values in literature for BASF $Cu/ZnO/Al_2O_3$ catalysts.

$$\rho_{MgO_r}(kg/m^3_{reactor}) = \rho_{MgO}(kg/m^3_{MgO}) \cdot \epsilon \tag{16}$$

$$V_{reactor} = \frac{F_{MeOH_{in}} \cdot (\frac{W}{F})}{\rho_{MgO_r}} \tag{17}$$

PSA Sizing

From the diameter and length obtained previously, and the adsorption capacities of the adsorbent, one could calculate the saturation time. A design procedure following McCabe and Smith is used [40]. As the maximum adsorption capacity, W_{sat}, is known from the publication by Agueda et al. [7], Equation 18 can be used to calculate the saturation time needed based on the length of bed, density of the adsorbent, superficial velocity (set to 0.1 m/s), and the initial concentration of the impurity at the entrance of the bed, which is obtained from Aspen Plus.

$$t^* = \frac{L \times \rho_{adsorbent} \times W_{sat}}{u \times c_{i,0}} \tag{18}$$

Table 16 gives an approximate estimation of the saturation time for CO and CO_2. Note that the multi-component adsorption effect is not taken into account in this case.

Another aspect to consider is the pressure drop across the column. In industrial applications, a 0.2 bar pressure drop is the maximum to accept. The length that is needed to exceed the pressure drop limit is around 100 m for the feed properties displaced in Table 17. This was calculated using Equations 19, 20, 21.

Table 16: Saturation Time for CO_2 and CO.

Parameter	**CO_2**	**CO**
W_{sat} (mol/kg)	4	2.5
$c_{i,0}$ (mol/m^3)	123	23.2
t* (hours)	1	0.94

$$Re = \frac{d_p \cdot u}{\mu_{mix}} \tag{19}$$

$$f_m = \frac{100}{Re} \tag{20}$$

$$L = \frac{d_p \cdot \epsilon^3 \cdot \Delta P}{2u^2 \cdot (1-\epsilon)^3 \cdot f_m} \tag{21}$$

Table 17: Properties of PSA Feed Mixture: Obtained from Aspen Plus.

Parameter	**Value**
Mass Flowrate (kg/h)	6482
d_p (mm)	2
ΔP_{max} (Pa)	20000
μ_{mix} (Pa·s)	1.17×10^{-5}
ϵ_v	0.4
$\rho_{mixture}$ (kg/m^3)	9